A Synoptic–Dynamic Model of Subseasonal Atmospheric Variability

KLAUS WEICKMANN

Physical Sciences Division, NOAA/Earth System Research Laboratory, Boulder, Colorado

EDWARD BERRY

National Oceanic and Atmospheric Administration/National Weather Service, Dodge City, Kansas

(Manuscript received 5 October 2005, in final form 3 May 2006)

ABSTRACT

A global synoptic–dynamic model (GSDM) of subseasonal variability is proposed to provide a framework for real-time weather–climate monitoring and to assist with the preparation of medium-range (e.g., week 1–3) predictions. The GSDM is used with a regional focus over North America during northern winter. A case study introduces the time scales of the GSDM and illustrates two circulation transitions related to eastward-moving wave energy signals and their connection to remote tropical forcing. Global and zonal atmospheric angular momentum (AAM) is used to help define the synoptic evolution of the GSDM components and to link regional synoptic variations with physical processes like the global mountain and frictional torque. The core of the GSDM consists of four stages based on the Madden–Julian oscillation (MJO) recurrence time. Additionally, extratropical behaviors including teleconnection patterns, baroclinic life cycles, and ~monthly oscillations provide intermediate and fast time scales that are combined with the quasi-oscillatory (30–70 day) MJO to define multiple time-/space-scale linear relationships. A unique feature of the GSDM is its focus on global and regional circulation transitions and the related extreme weather events during periods of large global AAM tendency.

1. Introduction

Background

Synoptic models of atmospheric phenomena and dynamical or physical processes have been used extensively to communicate the results of diagnostic research and to help develop the science and art of weather forecasting. The extratropical cyclone and its baroclinic–barotropic life cycle is the most well known subject of synoptic modeling in meteorology. It has been studied with numerical models and observed datasets for more than 70 yr (e.g., Bjerknes 1919; Rossby 1941; Shapiro and Gronas 1999). Coherent and easily recognized, the behavior of baroclinic waves is the "bread and butter" of short-term prediction models, which have very good forecast skill in the 1–3-day range, at least on average (Simmons and Hollingsworth 2002).

Corresponding author address: Dr. Klaus Weickmann, Physical Sciences Division, NOAA/Earth System Research Laboratory, R/PSD1, 325 Broadway, DSRC-1D125, Boulder, CO 80305-3337. E-mail: klaus.weickmann@noaa.gov

DOI: 10.1175/MWR3293.1

No comparable synoptic model exists for subseasonal (3–90 days) variability and medium-range predictions. In fact, several additions to the baroclinic life cycle model would be required to construct a "useful" medium-range synoptic model. For one, the regional domain of the short-term prediction problem is no longer adequate for the medium range (e.g., Smagorinsky 1967). Wave packets or other organized atmospheric energy pulses can spread signals from regional tropical-extratropical interactions around the hemisphere in <10 days (Chang 1993, 1999a,b). The inherent scales of motion are also larger, in particular encompassing zonal wavenumbers 0–3. In the time domain, the model should consist of multiple time scales and their interactions in time and space. In terms of coherent phenomena, the quasi-oscillatory Madden–Julian oscillation (MJO; Madden and Julian 1971, 1972, 1994) is a viable candidate to provide structure to a global subseasonal synoptic model in the same way that El Niño–Southern Oscillation (ENSO) does for interannual variability. But the MJO is far from adequate by itself. Extratropical phenomena must also be included.

Historically, the most well-known extratropical variations are baroclinic waves, "blocking," and zonal index cycles (e.g., Namias 1954). The latter involve hemispheric variations between blocked and strong zonal flows. In modern times, teleconnection patterns (Wallace and Gutzler 1981, hereafter WG81; Branstator 1992) have been recognized as a general mode of circulation variability, of which blocking is a special case (Dole 1986, 2007). More recently, zonal mean or "annular" modes of variability are again being highlighted in diagnostic studies, especially those based on surface pressure or height (Thompson and Wallace 2000). Studies of the evolutionary behavior of zonal mean anomalies have revealed episodes of coherent propagation all the way from equatorial regions to high polar latitudes (Feldstein 2001). In the Southern Hemisphere, the MJO's quasi-stationary wave component (Weickmann et al. 1997, hereafter WKS) and a midlatitude component forced by baroclinic waves (e.g., Lorenz and Hartmann 2003) likely contribute to such episodes.

Although spatial differences are important, these phenomena all tend to be characterized by 5–10-day-decay time scales (Feldstein 2000) and by large zonal scales. Studies have sought to explain such low-frequency phenomena in terms of multiple equilibria (e.g., Charney and DeVore 1979) or normal modes (Simmons et al. 1983), although current evidence suggests that forcing helps determine their time behavior (Newman et al. 1997). Prominent forcing is supplied by the MJO, topography, the storm tracks, and sea surface temperature (SST) variations. A representative component from this class of red noise processes will make up the intermediate time scale of the global synoptic–dynamic model (GSDM). We specifically focus on a large-scale disturbance that develops over the Pacific–North American sector in association with orographically perturbed flow over the eastern Asian and western North American mountains and will refer to the phenomenon as the "$\tau_F - \tau_M$ index cycle."[1] Regionally it includes teleconnection patterns like the Pacific–North American pattern (PNA; WG81). Weickmann (2003, hereafter W03) has studied its synoptic evolution and Weickmann et al. (2000, hereafter WRP) argue that it is the dominant mode of atmospheric angular momentum (AAM) exchange and anomaly decay on intermediate subseasonal time scales.

The fast baroclinic life cycle has been studied for various background flows and meridional shears (Simmons and Hoskins 1978, 1979, 1980). Disturbance growth, phase propagation, energy dispersion, and breaking are prominent features of such studies (Thorncroft et al. 1993; Whitaker and Sardeshmukh 1998) and of the observed atmosphere. Regional baroclinic wave breaking (Nielsen-Gammon 2001) in particular produces a rapid meridional momentum exchange that influences even the zonal mean zonal wind. The residual of breaking waves has recently been linked with the initiation of teleconnection patterns like the North Atlantic Oscillation (NAO; Franzke et al. 2004). The fast time scale of the GSDM will focus on wave energy dispersion that accompanies baroclinic developments and their interaction with the major mountain ranges.

Specifically, synoptic-scale wave energy dispersion within the northern and subtropical waveguides over Asia and the Pacific Ocean (Hoskins and Ambrizzi 1993; Chang 2005) will represent the model's fast time scale. The process is linked with 10–30-day oscillations of the circulation, which have been observed throughout the atmosphere. Wave retrogression at high northern latitudes (Branstator 1987), mountain torques over Asia and North America (Lott et al. 2001; Lott and D'Andrea 2005), equatorial convectively coupled Rossby and Kelvin waves (Wheeler et al. 2000), and monsoon oscillations (Hartmann et al. 1992) all display coherent behavior on this time scale. This component can be energetic for an extended time period as during the 1996–97 rainy season over central California (Mo 1999). The specific ~25-day oscillation represented in the GSDM involves subtropical flow variations, a likely candidate for the behavior described by Mo (1999). Mo (2001) has incorporated the intermediate time scale explicitly into the week 1–3 prediction process.

The GSDM organizes these multiple subseasonal phenomena into a repeatable sequence. The relationship among the time scales is based on maximizing global and zonal AAM anomalies. The GSDM emphasizes four primary stages but the duration of the cycle and the days between stages are variable. The model is valid during persistent forcing by sea surface temperature anomalies as well as during the time-varying MJO. In fact, two of the stages represent behavior also observed during El Niño and La Niña events. The GSDM is similar to using composites of ENSO or MJO for real-time monitoring and seasonal or weekly predictions, although we seek to explain and account for more variance through the multiple time-scale approach.

[1] A zonal index fluctuation with a broad anomaly center in the Tropics (30°N–30°S) and an opposite-signed anomaly at 50°N. The pattern is amplified and extended in time by the meridional transports of AAM associated with Rossby wave trains that induce a large Northern Hemisphere mountain torque. The zonal wind anomalies eventually decay via the frictional torque.

A dynamical underpinning for the model is atmospheric angular momentum, which is determined by the three-dimensional distribution of atmospheric zonal wind and mass (Peixoto and Oort 1992). Its global integral is an excellent index of ENSO, the MJO, and other subseasonal variability. Moreover, processes that change global AAM, that is, the frictional torque and the mountain torque, have medium and fast time scales, respectively (WRP). Thus, indices involving these processes are used to define the components of the GSDM. WRP show that the mountain torque forces AAM anomalies and the frictional torque damps them (Egger and Hoinka 2002), and this will be evident in the GSDM. Atmospheric dynamics linked with wave growth and dispersion processes connect the mountain source regions of AAM anomalies with the subtropical frictional sink regions. The latter tend to occur near the seasonally varying zero zonal wind line. The torques are produced by a variety of known, large-scale patterns of wind and pressure as described by WRP and W03.

There are two primary motivations for the synoptic modeling effort. The first is scientific understanding of the evolving atmospheric circulation with a practical goal of attribution of weather–climate anomalies. Diagnostic tools and analysis results derived from the science and research side are used on the monitoring and prediction side to examine cause and effect or the attribution of weather climate variations. The application of diagnostics to actual forecasting is mostly neglected in meteorology because of the strong reliance on numerical forecast models and lack of a useful synoptic framework. The second motivation is daily monitoring of the circulation to evaluate numerical model predictions in the subseasonal band, including the potential predictability of transitions of the circulation and of extreme weather events. Extreme events of global AAM are used as a framework within the GSDM. The specific intent is to target the boundary between weather and climate, which encompasses the transition from deterministic to probabilistic forecasts. An evaluation of numerical forecasts based on synoptic reasoning is expected to add value because there are well-known, stubborn model errors, particularly in the prediction of tropical convection (Lin et al. 2006) and the subsequent circulation response.

Section 2 introduces aspects of the GSDM with a case study presentation of the 2001–02 northern winter season. Two rapid transitions of the circulation that involve tropical–extratropical interaction are described, as well as the predictive skill of an ensemble forecast model. The derivation of the GSDM is then presented in section 3. The evolving circulation anomalies of the different components of the synoptic model are organized using a linear superposition based on the time tendency of global relative AAM. A summary and conclusions follow in section 4.

2. A case study: December 2001–February 2002

The purpose of this case study is to introduce phenomena and variability that will be used to construct the GSDM. Two transitions of the circulation will be examined that occur in association with two moderate MJOs. The case begins in a low AAM state typical of a La Niña circulation regime. A transition then occurs to a high AAM state typical of El Niño, and the case ends with a transition back to a La Niña state. The use of the ENSO cycle to describe subseasonal variations of the circulation and convection emphasizes the strong similarity between the responses to tropical convection on interannual and subseasonal time scales. In fact, stages 1 and 3 of the GSDM, which are introduced in the next section, closely resemble the well-known La Niña and El Niño circulation anomalies, respectively. In the following, when we will refer to stage 1 and stage 3, the reader should know what we mean. The other outstanding forcing during the case was by the mountain torque, which represented the other two time scales of the GSDM reasonably well. The fast time scale will be obvious but the intermediate time scale is represented because regressions on the daily frictional torque closely resemble regressions on 5–7-day means of the mountain torque (not shown). To focus the study, the roles of the MJO convective signal, the midlatitude mountain torque, and synoptic-scale wave trains are described during two transitions of the large-scale flow.

The MJO activity during 2001–02 not only influenced the tropical convection and circulation during the study period but also the SST anomalies in the tropical Indo-Pacific Ocean. SST anomalies were recovering from a series of weak–moderate La Niñas in the previous 3 yr and, during northern fall 2001, positive SST anomalies were found in the tropical west Pacific Ocean. The first MJO during November 2001 helped force a shift of the ocean warm pool farther eastward toward the date line. This SST change led to a "regime" of ~25-day tropical convective variability over the west Pacific Ocean—a good example of the behavior described by the <30-day filtered global relative AAM tendency used in the GSDM.

a. Tropical convection

The two MJOs are shown in a time–longitude format in Fig. 1. MJO 1 forms over the Indian Ocean in November 2001, shifts to the west Pacific in early December

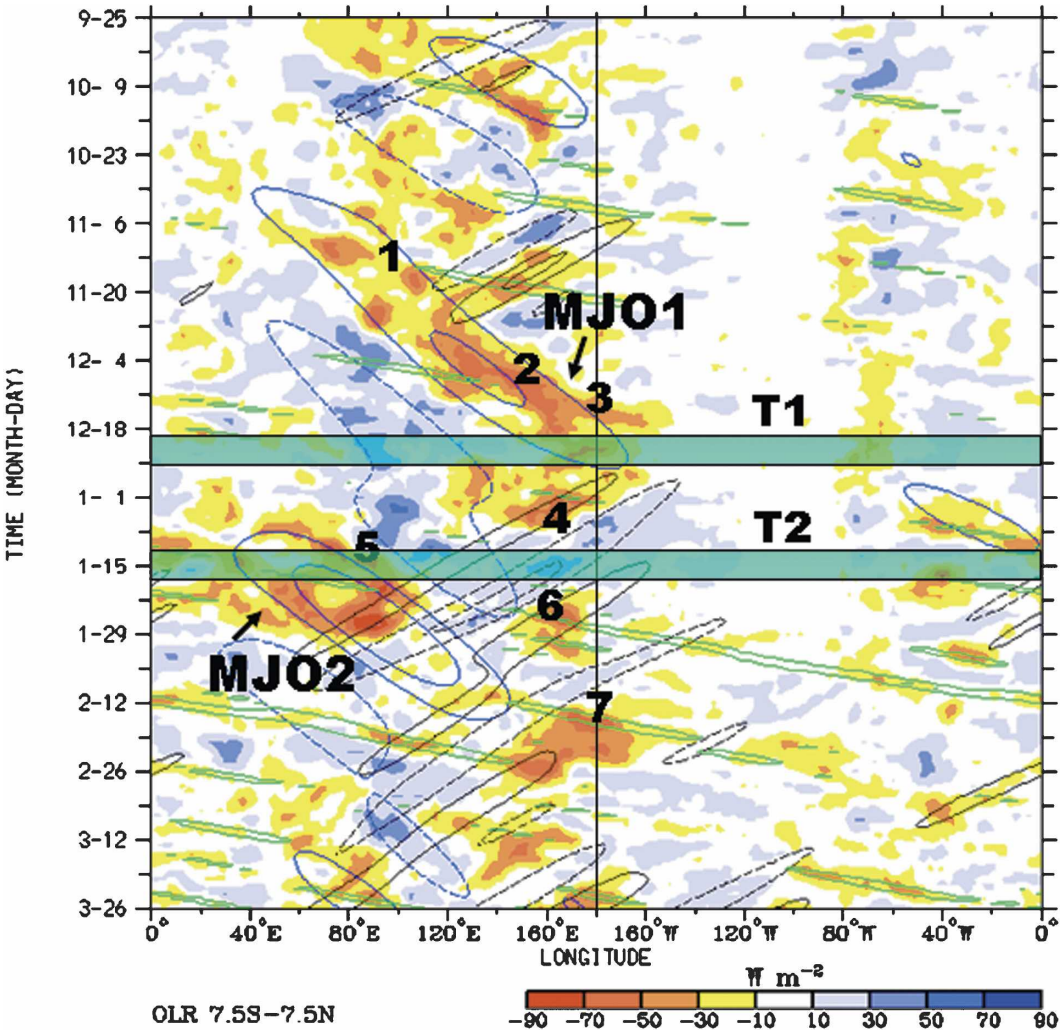

FIG. 1. Hovmöller plot (time–longitude section) of OLR anomalies averaged between 7.5°N and 7.5°S, where the contours illustrate space–time-filtered coherent tropical convection modes for 25 Sep 2001–26 Mar 2002. The blue contours represent the MJO (solid blue for enhanced convective phase, dashed for suppressed phase). The green contours are for Kelvin waves and the brown contours isolate an equatorial Rossby mode. See Wheeler and Kiladis (1999) for additional details. MJOs 1 and 2, T1 and T2, and the 1–7 numbering refer to important developments discussed in the text and listed in Table 1. The lightly shaded horizontal bars highlight the transitions for the case study, with T1 (T2) from 19–25 Dec 2001 (12–18 Jan 2002).

2001, and stalls west of the date line. The stalling may reflect a feedback from the eastward shift of warm ocean water cited above. MJO 2 forms over the Indian Ocean in mid-January 2002 and reaches the date line in mid-February. It contains more Kelvin and equatorial Rossby wave activity than MJO 1 and has its convective signal south of the equator for most of February 2002 (see Fig. 1). Both MJOs have significant amplitude in the filtered field, especially at ~120°E. Using this longitude as a reference gives a recurrence interval of 65 days, which is on the long end of the MJO period range.

To start the process of telescoping to the two transitions and their link to MJO-related convective forcing, seven numbers have been marked on Fig. 1. These numbers "sample" rapid changes within the two MJOs' convective envelope and in the ~25-day quasi oscillation along 160°E. They will be referred to as "tropical convective flare-ups." The dates for the flare-ups were determined from a time series of the first 2 EOFs of 20–100-day filtered outgoing longwave radiation (OLR) anomalies (shown below). The two GSDM transitions are associated with flare-ups 3 and 5. Here, T1 represents the transition to stage 3 (i.e., like El Niño) when MJO 1 is located over the west-central Pacific, and T2 is the transition to stage 1 (i.e., like La Niña) when MJO 2 is over the Indian Ocean. Table 1

TABLE 1. Key dates during the case study. Events 1–7 are tropical convective flare-ups while T1 and T2 are circulation transitions.

No.	Event
1	6 Nov 2001: persistent eastern Indian Ocean convection from boreal fall 2001 evolves into MJO 1
2	4 Dec 2001: MJO 1 moves into western Pacific Ocean
3	10 Dec 2001: MJO 1 moves to date line and convection then persists for roughly 20 days over relatively warm SSTs (~+0.5°–1.0°C anomalies). Convection is generally suppressed across Indian Ocean during this time
4	5 Jan 2002: enhanced convection finally ends west of the date line. A series of convectively coupled equatorial Rossby waves start to move west from the central Pacific to Africa
5	10 Jan 2002: enhanced convection over the Indian Ocean evolves into MJO 2
6	20 Jan 2002: convection again flares up in the equatorial date line region (~160°E). This area persists for about 10 days while MJO 2 is farther west and moving east
7	10 Feb 2002: enhanced convection develops across the equatorial date line region in association with MJO 2
T1	Transition 1, for 19–25 Dec 2001. The circulation of the atmosphere shifts to GSDM stage 3, a response to enhanced central Pacific tropical forcing initiated by flare-up 3 on 10 Dec 2001
T2	Transition 2, from 12–18 Jan 2002. The atmospheric circulation shifts back to GSDM stage 1, a response to the reversal of the tropical convective forcing shown by flare-ups 4 and 5

gives the calendar dates corresponding to the numbered events and the two transitions. Although only flare-ups 3 and 5 are studied in what follows, the other cases also produced regional and downstream transient impacts on the atmospheric circulation and on weather-producing disturbances.

b. Midlatitude 250-mb meridional wind

The midlatitude circulation anomalies that accompany the tropical OLR signal are depicted using a daily time-longitude plot. Figure 2 shows the 250-mb meridional wind anomalies averaged between 30° and 60°N and depicts (i) signatures of storms in the storm-track regions, (ii) energy dispersion in midlatitude regions, and (iii) slow, quasi oscillations in the midlatitude meridional wind pattern. The latter will be discussed in terms of the implied geopotential height anomalies, which are marked on the figure. These height patterns involve ridging near 150°W (Hs) during the first half of December 2001, troughing in the same location (Ls) during the rest of December into early January 2002, and a return to ridging (Hs) in mid-January–early February 2002. Each persistent episode includes 3–5 synoptic-scale events whose ridges and troughs tend to develop or amplify at the same longitude. The synoptic events have been numbered for each of the three persistent "regimes."

The boundaries of T1 and T2 are marked on Fig. 2 and a wave train that extends from 120°E to 90°W is highlighted during each transition. The wave trains are linked with the retrogression of existing anomalies (red arrows) and are followed by a series of similar synoptic events. After T2 and the return of ridging to the eastern North Pacific, the synoptic activity is more spatially variable than during stage 3. It also includes a slow westward drift of the circulation anomalies (light dashed lines) at a time when positive tropical convection anomalies are over the Indian Ocean and Indonesia. The final synoptic regime seen in Fig. 2 is a progressive one (light solid lines), which coincides with the return of convection to the date line around 12 February 2002.

c. Low-frequency indices and their forcing

Figure 3 shows daily indices that capture the low-frequency (>10 day) variations described in Fig. 2 and illustrate the atmospheric response to tropical diabatic heating and orographic forcing to be detailed later. The indexes include (i) the global integral of AAM, (ii) the first EOF of the combined 200-/850-mb vector wind field (with the zonal mean removed), and (iii) the PNA teleconnection pattern. These represent global, hemispheric-subtropical, and regional anomaly patterns, respectively. All have similar low-frequency behavior, that is, minima in early December 2001 (day 30), maxima in late December–early January 2002 (day 60), and back to minima in late January 2002 (day 80). The center of transitions T1 and T2 are again marked on the curves. The PNA slightly lags the other curves, which is consistent with a signal that starts in the Tropics, expands to the subtropics, and eventually affects the regional circulation over the midlatitude Pacific Ocean.

The time series of processes that can force these changes are depicted in Fig. 4. Figure 4a shows the first EOF of the zonal mean mountain (red) and frictional torque (blue) over the Northern Hemisphere. EOF 1 of the mountain torque (not shown) is a monopole pattern between 20° and 60°N, and EOF 1 of the frictional torque (not shown) is a north–south shift in the winter mean boundary of the surface westerly flow. Figure 4b shows coefficients of the first two EOFs of OLR, which describe an eastward movement of the MJO. The convective flare-ups numbered in Fig. 1 (see also Table 1)

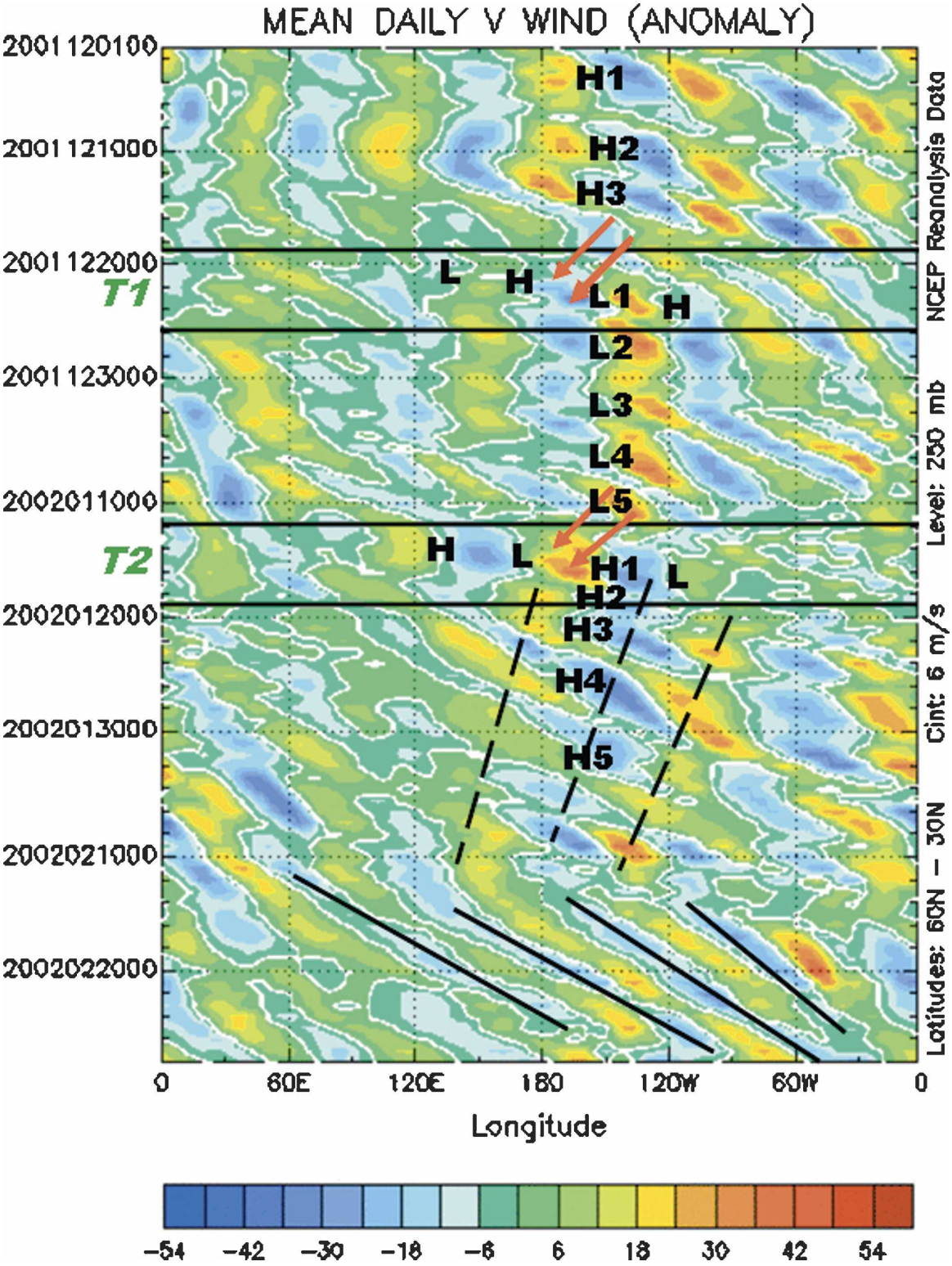

FIG. 2. Hovmöller plot of 250-mb meridional wind anomalies averaged from 30°–60°N during the period of 1 Dec 2001–28 Feb 2002. The solid horizontal lines depict the periods for T1 and T2, and the "Hs" and "Ls" highlight positions of anomalous synoptic-scale ridges and troughs, respectively. The red arrows indicate the retrogression of existing anomalies while the light dashed lines show a slow westward regime shift. The slanted solid black lines indicate progressive circulation anomalies after 1 Feb 2002.

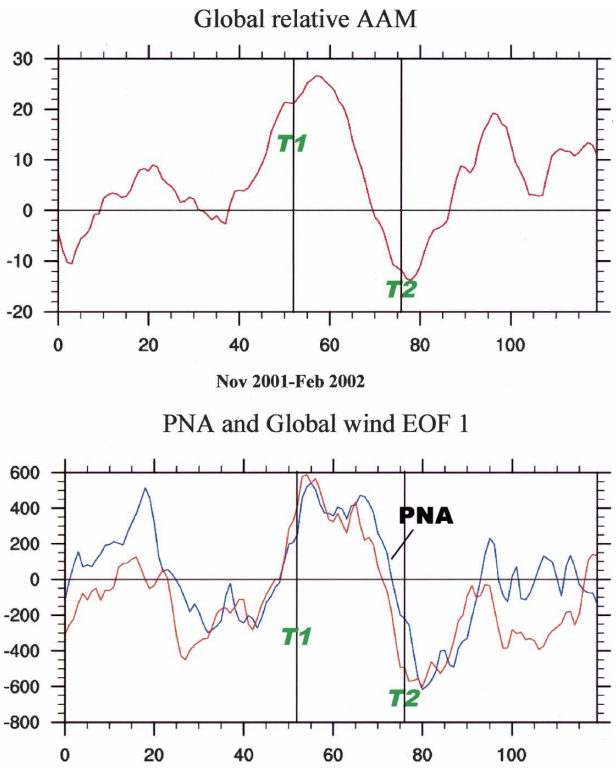

FIG. 3. Time series plots of indices describing low-frequency variations for the period of 1 Nov 2001–28 Feb 2002. The days are on the abscissa, where day 0 is for 1 November, and increasing from left to right. The numbers on the ordinate are (top) AAM units = 1.0×10^{24} kg m^2 s^{-1} and (bottom) dimensionless measures of amplitude. The (top) is for the global integral of AAM while the (bottom) shows the plots for the first EOF of the combined 200–850-mb vector wind field (red) and the PNA (blue). The vertical lines depict the center date for T1 and T2.

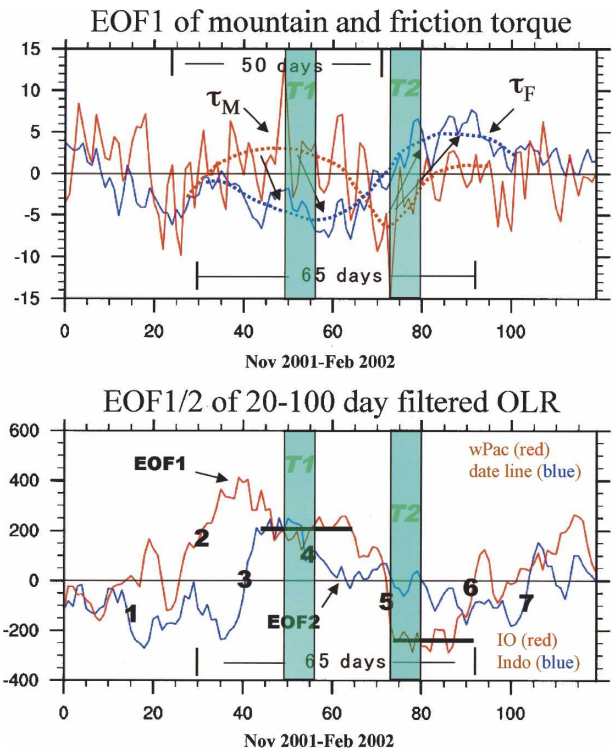

FIG. 4. Time series plots for the period of 1 Nov 2001–28 Feb 2002 (see Fig. 3). (top) The first EOF of the zonal integral of the mountain and frictional torque (red is mountain torque, blue is frictional torque) and (bottom) the first 2 EOFs of 20–100-day filtered OLR (red is EOF 1, blue is EOF 2). The text on the right indicates the location of anomalous convection corresponding to positive and negative values of each EOF. The Indian Ocean is represented by IO. Shaded vertical bars represent T1 and T2.

were derived from these OLR EOFs and are also marked.

These forcing time series have some distinct low-frequency behavior in addition to the rapid convection changes seen in Fig. 4b and the highly variable synoptic component seen in the mountain torque time series of Fig. 4a. From Fig. 1, a 65-day recurrence interval for MJO convection was estimated for 120°E; this is marked at the bottom of Figs. 4a,b. Negative values of OLR EOF 2 are seen at the endpoints of the interval in the lower panel and signify that convection is indeed located over Indonesia at these times. More generally, OLR EOF 1 (red) leads EOF 2 (blue), consistent with the eastward propagation of anomalies.

Another low-frequency behavior marked on Fig. 4a is a 50-day recurrence interval in the midlatitude mountain torque (Lott et al. 2001). As mentioned previously, the frictional torque (Fig. 4a) acts to damp angular momentum anomalies forced by the mountain torque, but it is also involved in producing the MJO AAM signal. In the GSDM, the MJO, intermediate ~6-day decay time scale, and 10–30-day oscillation can contribute to circulation anomalies during stages 1 and 3. These phenomena are difficult to disentangle since in all, a positive mountain torque is followed by a negative friction torque and vice versa. A section of each time series has been highlighted with a dotted line that shows this lag relationship for a ~50-day oscillation. It is perhaps clearest after T2. Namely, as the large negative mountain torque removes westerly momentum from the atmosphere, easterly wind anomalies and a positive friction torque develop. This slowly removes easterly momentum from the atmosphere, thereby bringing AAM back into temporary balance. It is during this damping process that circulation anomalies of interest to monitoring and prediction occur, in this case a negative PNA. Another example but with opposite sign is also highlighted during December 2001 on Fig. 4a with two black arrows.

The locations of T1 and T2 are marked with shading on Fig. 4. The transitions follow closely the very large positive and negative maxima in the mountain torque anomaly, which are embedded in strong daily variability as synoptic systems move over the topography. Asian–European topography is a strong contributor to both the positive and negative anomaly while North American topography contributes primarily to the later negative anomaly (not shown). The mountain torque events are linked with the amplification of a baroclinic wave downstream of the Asian topography over the western half of the North Pacific. During T1, the amplifying wave leads to a cyclonic wave break over the east Pacific that brings westerlies south and ushers in stage 3. The opposite happens during the transition to stage 1.

Figure 4b shows that the transitions occur 5–10 days after flare-up 3 and 1–3 days after flare-up 5. This suggests a loose relationship between rapid transitions in the circulation and the sudden shift of convection within the MJO convective envelope. In this case, it is the midlatitude mountain torque that is more directly linked with both transitions. However, the persistence of tropical forcing, as represented by the heavy horizontal bars on the EOF 1 OLR time series, undoubtedly contributed to the persistence of the resulting large-scale circulation anomalies.

d. Synoptic maps during circulation transitions

Figure 5 shows selected daily maps of the 150-mb vector wind anomaly during T1. The key anomalies from an MJO perspective are suppressed convection over the Indian Ocean and active convection near the date line (not shown, but see Fig. 1). Early in the sequence (Figs. 5a,b), a wave train is evident across the Indian Ocean/south Asia with a trough near 20°N, 70°E. The trough is quasi-stationary and eventually evolves into a large cyclonic anomaly covering the entire region (Fig. 5f). The MJO at this stage helps force the trough and sets the phase of a wavenumber 5–6 wave train through which energy flows eastward. Another more stationary wave train farther north (60°N) combines with the subtropical wave train over the midlatitude North Pacific in Fig. 5b, which precedes the wave amplification over the west Pacific seen in Figs. 5d–f. The phase of the amplifying couplet west of the date line is consistent with the orographic response to a positive mountain torque (W03). Baroclinic processes and upper-level outflow from the tropical convection west of the date line help the amplification process. In Fig. 5f, the downstream low over the northeast Pacific has developed a negative tilt, and a full cyclonic breaking event is in progress. This behavior also becomes linked with a retrograding anticyclonic anomaly across Canada and the North Atlantic, which allowed for a strong projection onto the positive phase of the PNA and the negative phase of the NAO. This pattern of strong tropical–subtropical westerlies stays in place for ~15 days.

Almost the opposite behavior was observed during T2, whose synoptic evolution to GSDM stage 1 is shown in Fig. 6. Now instead of a trough, there is a ridge at 20°N, 70°E (Figs. 6a,b), which is being forced by the strong convection over the Indian Ocean. The phase of the wave train is reversed compared to Fig. 5, and the Indian Ocean ridge grows into a large anticyclonic anomaly over south Asia as the transition matures (see Fig. 6f). The downstream amplification over the west North Pacific also occurs, but with the phase reversed (Figs. 6b–d) and little evidence of a preexisting wave train farther north. This leads to a wave break over the east Pacific (Figs. 6e,f) that becomes anticyclonic along the U.S. west coast. The stage 1 pattern was maintained by additional meridional–zonal flow variations leading to more anticyclonic wave breaking along the U.S. west coast (not shown). The final wave break occurred during late January 2002 and linked up with an anomalously strong subtropical jet, forced by tropical convective flare-up 6 near the date line, to produce an extreme winter weather event (snow and freezing rain) over the Great Plains. The GSDM stage 1 characteristics of the circulation finally broke down in mid-February 2002 (see Fig. 2).

e. Predictive skill of circulation transitions

The abrupt onset of the stage 3 and stage 1 circulation regimes has forecast implications for the medium range. Figure 7 shows the ensemble mean forecast skill out to day 15 during the 2001–02 winter season using a 1997 version of the National Centers for Environmental Prediction (NCEP) Medium-Range Forecast model. This model has a 25-yr reforecast dataset available and real-time predictions are posted on the Web (Hamill et al. 2004; see http:www.cdc.noaa.gov/people/jeffrey.s.whitaker/refcst/week2/). The skill measure used here is the spatial correlation between verifications and predictions of Northern Hemisphere 150-mb streamfunction anomalies. There are 3 periods where the 11-day ensemble-mean forecast skill of the Northern Hemisphere 150-mb streamfunction anomaly is relatively poor (<0.5). The common thread in these low-skill regimes is that a major change in tropical convective forcing is observed (and presumably not captured) during the forecast cycle. The major convective changes are highlighted with arrows in the top panel of Fig. 7

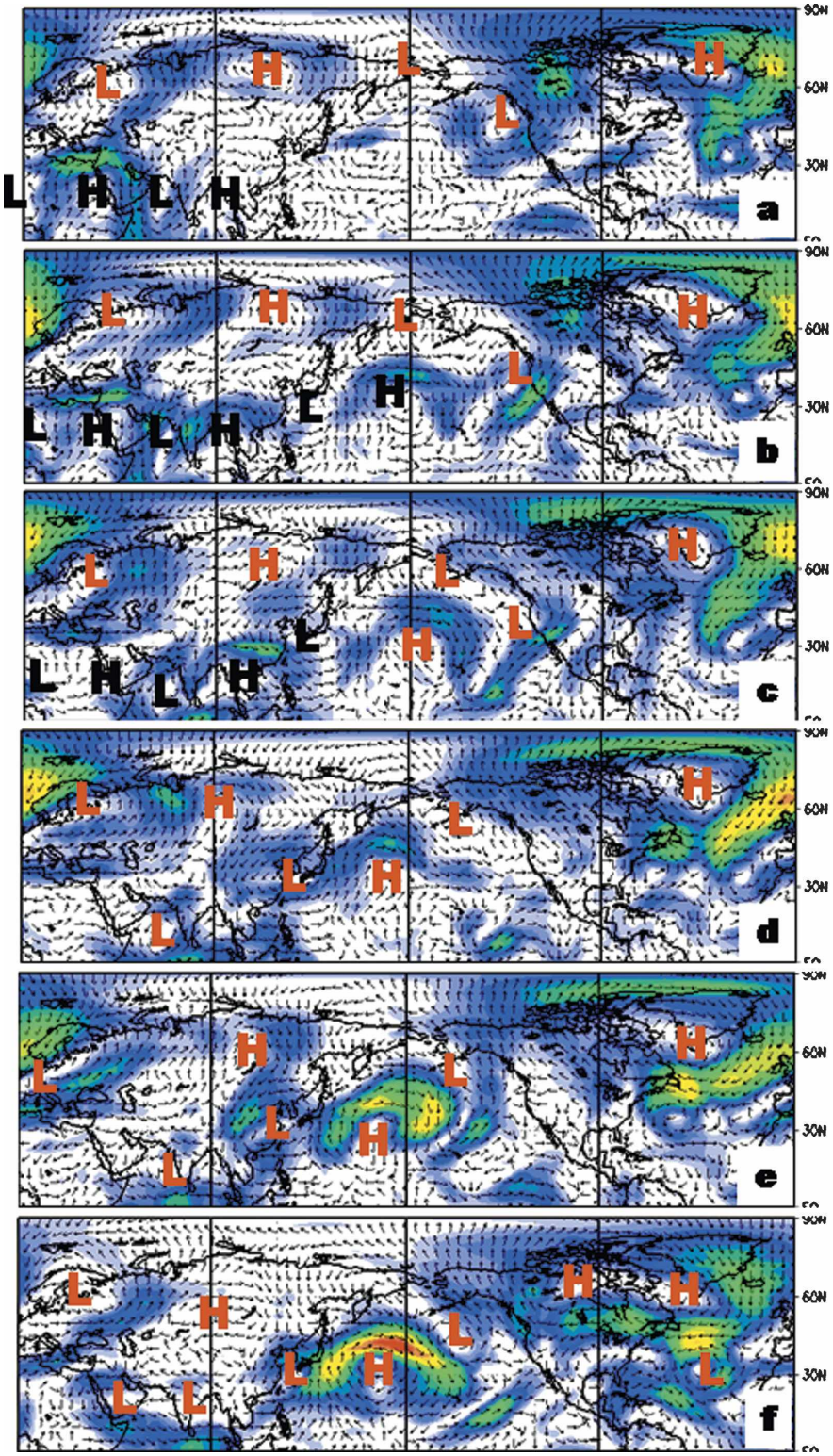

FIG. 5. The daily evolution of 150-mb vector wind anomalies for T1, the transition to stage 3 of the GSDM. Here, Hs and Ls refer to anomalous anticyclonic and cyclonic circulations. The dates are (a)–(f) 19, 20, 21, 22, 23, and 25 December, respectively. The vertical lines highlight 90°E, 180°, and 90°W.

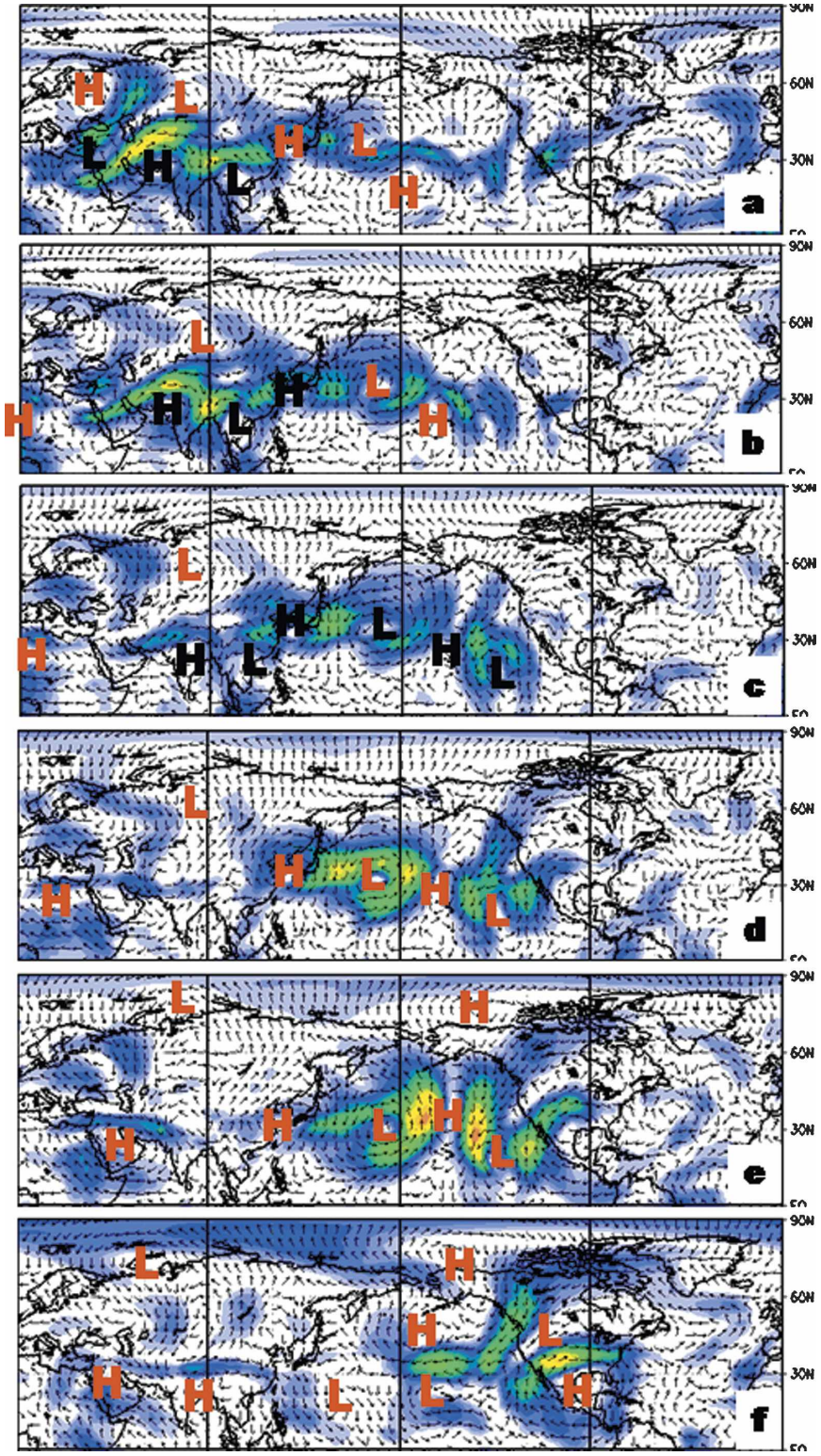

FIG. 6. Same as in Fig. 5 but for T2, the transition to stage 1 of the GSDM. The dates are (a)–(f) 12, 13, 14, 15, 16, and 18 January, respectively.

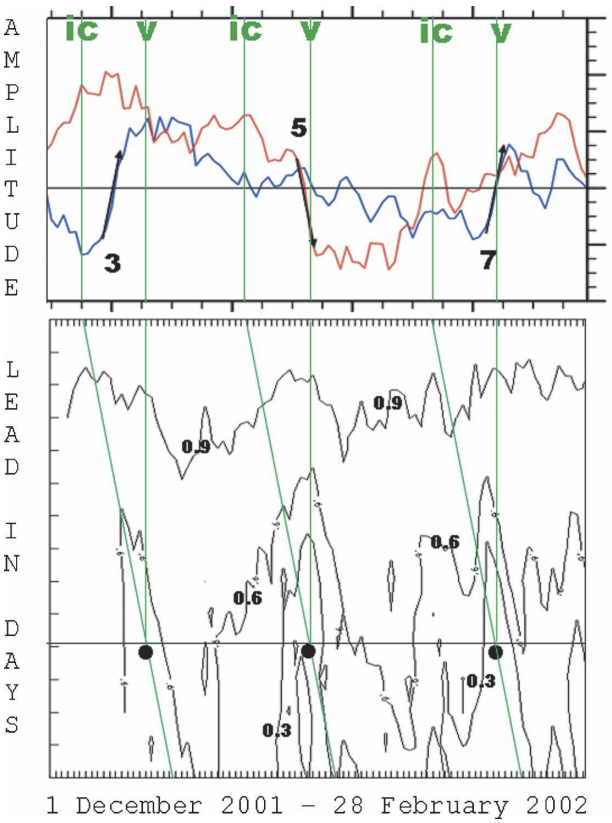

FIG. 7. (top) Time series plots of OLR EOFs 1 and 2 (as in Fig. 4) and (bottom) forecast skill for a forecast model ensemble mean during the period of 1 Dec 2001–28 Feb 2002 (abscissa, days increasing from left to right). Here, "IC," "V," and the vertical lines highlight the model initial condition and verification times for the three cases discussed in the text. Forecast skill is expressed in terms of the anomaly correlation coefficient over the entire Northern Hemisphere of 150-mb streamfunction. The contour interval on the (bottom) is 0.3 and the black dots show the dates of the lowest day 11 forecast skill. The slanted lines indicate the model forecast cycle (day 1–15 lead) for three cases, including T1 and T2. The horizontal line highlights the day 11 lead.

(i.e., flare-ups 3, 5, and 7). Note that the 5 and 7 transitions occur near the end of the forecast cycle, implying a rapid impact on the circulation anomalies of the Northern Hemisphere, if indeed they are the cause for the low forecast skill.

For T1 and T2, the amplification of a wave disturbance over the western North Pacific is a key synoptic event. On 23–24 December 2001, the "low–high" couplet west of the date line (Fig. 5d) was predicted 11 days in advance but the "high–low" couplet in the same place on 15–16 January (Fig. 6d) was not. A clue about what may be happening is derived from the general pattern of forecast skill described above for the 2001–02 winter. The forecast for 23–24 December 2001 is initialized after flare-up 3 while the forecast for 15–16 January 2002 is initialized before event 5. Failure to capture the start of flare-up 5 and the large negative mountain torque in the forecast cycle presumably contributed to the low forecast skill during the second transition. Many more cases need to be examined to confirm these assertions.

f. Discussion

Several atmospheric phenomena and processes were introduced during the case study description. Tropical convective forcing involved multiple time scales including the 30–60-day MJO, 20–30-day convective flare-ups, and other convectively coupled equatorial waves. Topographic forcing from synoptic-scale disturbances was clustered on a 50-day time interval and produced zonal momentum anomalies that were removed by the frictional torque. The PNA teleconnection pattern was involved in the removal process. Finally, the phase of synoptic-scale wave trains over the Asian–Pacific sector was related to tropical convective forcing over the Indo-Pacific warm pool region and to subsequent anticyclonic and cyclonic wave breaking over the eastern North Pacific.

The 50-day "oscillation" in the mountain torque is consistent with the 6-day decay time scale of the $\tau_F - \tau_M$ index cycle. A red noise process with a 6-day decay time has its variance concentrated in a band with periods at around 6 days $\times$ 2π = ~38 days. Plotting its spectrum with the log of frequency as the abscissa in a variance-conserving format shows this feature of red noise most clearly (see, e.g., Fig. 2 of WRP). A 50-day oscillation is a representative example from such a process, but of course no coherent forcing exists at 50 days or any other period in the red noise background.

In the case study, these and other processes are seen as working together to produce the evolving atmospheric circulation anomalies. The indices in Fig. 3 show a slow evolution while Fig. 2 has the transition occurring rapidly in association with synoptic-scale wave trains. The latter are seen as a mechanism for the spatial spreading of information about the changes in forcing from key regions around the hemisphere (e.g., western ocean baroclinic zones, tropical convective zones, and centers of low-frequency variability). Certainly, a fortuitous or random nature must be assumed about these fast (~30 m s^{-1}) eastward-moving disturbances and their role in the transitions of the circulation; that is, there is always another synoptic system or wave train that can play the transition role. After the transition, repeatable synoptic events were superimposed on the quasi-stationary flow, and these represent the opportunities for skillful extended forecasts of synoptic-scale behavior.

The basic perspective is that forcing is of primary importance for determining the evolution of the atmospheric circulation and that different sources of forcing produce circulation responses that combine linearly to produce the circulation anomalies at any particular time. Anomalies may be maintained by feedbacks but eventually they disperse as the forcing waxes and wanes, even when coupling from persistent SST anomalies is involved. This perspective is supported by Sardeshmukh et al. (1997), Newman and Sardeshmukh (1998), and Newman et al. (1997), who demonstrate the importance of forcing for the evolution of low-frequency circulation anomalies. The success of the Winkler et al. (2001, hereafter WNS) linear inverse model (LIM) of weekly circulation anomalies is based on the importance of tropical and other forcing as a source for week 1–3 predictive skill.

WNS's linear inverse model of 7-day averages has features in common with the GSDM introduced in the next section. The LIM has three optimal structures that undergo nonmodal growth over a wide range of truncations and maximized growth rates. Two optimals are linked with forcing from the MJO and ENSO while the third is a PNA pattern linked to eddy feedbacks in midlatitudes. The LIM is objective, so it can be used for dynamical feedback studies (WNS) as well as predictability studies (Newman et al. 2003).

The GSDM is subjective but includes a synoptic component and a submonthly oscillation in addition to the MJO and the PNA, arguably four "modes" versus three for LIM. Its dynamics are based on the terms in the global and zonal AAM budget. Meridional and vertical transports help produce the torques at the surface. A linear phasing of GSDM components is assumed, and this unites several time and space scales within the model. The model does not explicitly include ENSO, but knowledge of the ENSO cycle is critical when applying it in real time. Both models can be further extended and are tools for monitoring, attribution, and prediction. The GSDM is introduced next.

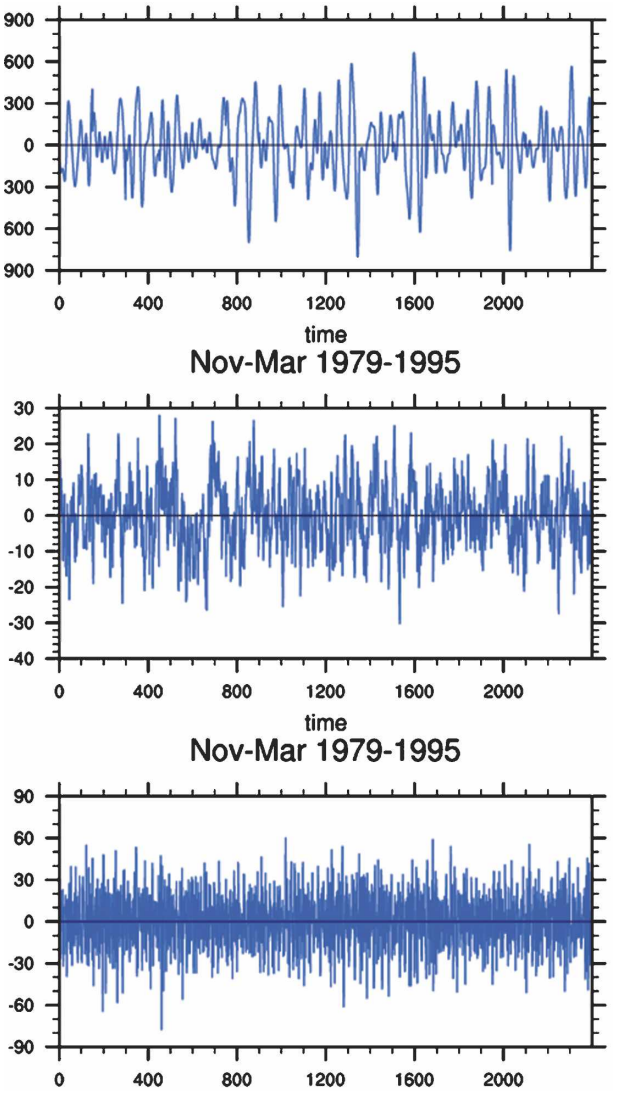

FIG. 8. Indices for 16 winter segments from November–March 1979–95. (top) The first EOF of 20–100-day filtered OLR represents the MJO, (middle) the daily global frictional torque with the MJO linearly removed represents teleconnection patterns, and (bottom) the <30-day filtered global relative AAM tendency represents wave energy dispersion over the mountains. The abscissas are time expressed as days while the ordinates are nondimensional measures of amplitude.

3. A Global Synoptic–Dynamic Model (GSDM) of subseasonal variability

The synoptic model organizes four subseasonal time scales into a single picture that describes a recurring evolution of global and regional weather climate patterns. Numerous indices could have been chosen to define a representative spatial evolution for each time scale. We use (i) the first EOF of 20–100-day filtered OLR to represent the MJO, (ii) the daily global frictional torque with the MJO linearly removed to represent the "τ_F–τ_M index cycle" (W03), and (iii) the <30-day filtered relative AAM tendency to represent wave energy dispersion over the mountains (W03) and 10–30-day oscillations. The indices are computed for the sixteen winter segments, November–March 1979–95. The segment mean is removed prior to the regression analysis to minimize contributions from interannual variability. Resulting anomalies will be interpreted relative to a smoothed seasonal cycle.

Figure 8 shows the three indices. Their different time behavior is self-evident and ranges from quasi-oscil-

latory (Fig. 8a) to red noise (Fig. 8b) to white noise plus a ~20–25-day oscillation (Fig. 8c).[2] We implicitly assume that these time scales are adequate to account for some interesting variations in the subseasonal band, with a focus over the Tropics, Asia, and the Pacific–North American region. First, however, we examine the relationship to global and zonal mean AAM, which are used to "phase" the model components.

a. Atmospheric angular momentum

In the case study, global AAM (Fig. 3) undergoes a relatively smooth evolution despite the complicated forcing depicted in Fig. 4. A careful examination of the AAM time series can discern the responses to the fast and medium excursions of the global mountain and frictional torques seen in Fig. 4, while the overall ~60-day oscillation implies a forcing by the weaker but more persistent torques associated with the MJO. Different time scales are clearly working together to produce the observed behavior. We now illustrate these building blocks and suggest why and how they may be related.

Figures 9b–d show the global and zonal AAM anomalies obtained when regressing onto the three indices of the GSDM in Figs. 8a–c. The heavy solid lines on Figs. 9a–e confirm that all three indices have a global AAM signal. The lag at which the AAM anomaly crosses 0 is ~+2 days (Fig. 9b), +7 days (Fig. 9c), and 0 days (Fig. 9d) for the 3 GSDM components. This is the key assumption made in constructing our model.[3] The point is that a linear combination of the three time scales, when shifted by these amounts, would result in a large relative AAM time tendency. We are specifically interested in large anomalies because synoptic experience indicates that extreme events consist of multiple time scales "working together." Such a linear combination would produce torques whose sum resembles the time series seen in Fig. 4a of the case study. Maximum AAM tendency would occur at stage 2 of the GSDM and would have contributions from all model components.

The zonal mean AAM anomalies when added depict a coherent signal of AAM anomalies moving out of equatorial regions toward the subtropics (Fig. 9a) and a weaker signal of anomalies moving equatorward around 50°N. The intermediate time scale $\tau_F - \tau_M$ index cycle (W03) imposes an asymmetry around day 0. Momentum transports by different types of eddies (e.g., subtropical wavenumber 1, midlatitude teleconnections, and midlatitude synoptic transients) play an important role in forcing all three of the zonal mean anomaly fields and provide a dynamical link between the time scales.

In the next subsection, the synoptic patterns related to the global and zonal AAM changes seen in Fig. 9 are presented. Since the <30-day tendency and the frictional torque regressions are performed on global indices, the results will emphasize those patterns that contribute to global AAM changes. For the <30-day tendency, the three main topographic regions are represented while for the global frictional torque, the Northern Hemisphere surface wind over both ocean basins will be important. During individual cases of subseasonal variation, not all regions will always contribute to the forcing. For example, in the case study, Asia was the primary contributor to the positive mountain torque before T1 while Asia and North America both contributed to the negative torque before T2. Nonetheless, a simultaneous forcing from the three regions is not unusual and can be organized by the poleward propagation of zonal mean wind anomalies or by the dispersion of Rossby waves into each hemisphere from west Pacific tropical heating. In general, however, the phasing of regional patterns is influenced by the use of a global measure on which to base the analysis and can distort important regional behavior.

b. Lagged regression sequences

Lagged linear regressions of global, 2D fields onto each index are used to define an evolution of circulation anomalies and will be referred to as a lagged regression sequence. Figures 10–12 show sequences 1–3 of 200-mb vector wind and sea level pressure (SLP) anomalies when regressed onto the 3 indices of Fig. 8. The duration and time interval of each sequence emphasize its time scale. Sequence 1 is 40 days long with a 10-day interval, sequence 2 is 18 days long with a 4-day interval, and sequence 3 is 8 days long with a 2-day interval. Global fields are shown because real-time monitoring suggests that coherent subseasonal interactions occur across broad latitudinal bands, often centered on either side of the equator. The sequences illustrate the well-known observation that large spatial scales coincide with long time scales. Beyond this, there are other features familiar to weather and climate scientists.

In sequence 1 (Fig. 10), the subtropical cyclones/anticyclones of the MJO are seen as they slowly propagate eastward from day −20 through day 0 to day 20. At day 0 (Fig. 10), convection is active over the equatorial

[2] A statistically significant ~25-day oscillation appears in the spectra of global relative AAM in 2 different 16-winter periods: 1962–78 and 1979–95.

[3] One could also use the time of maximum zonal AAM tendency at the equator and get slightly different numbers.

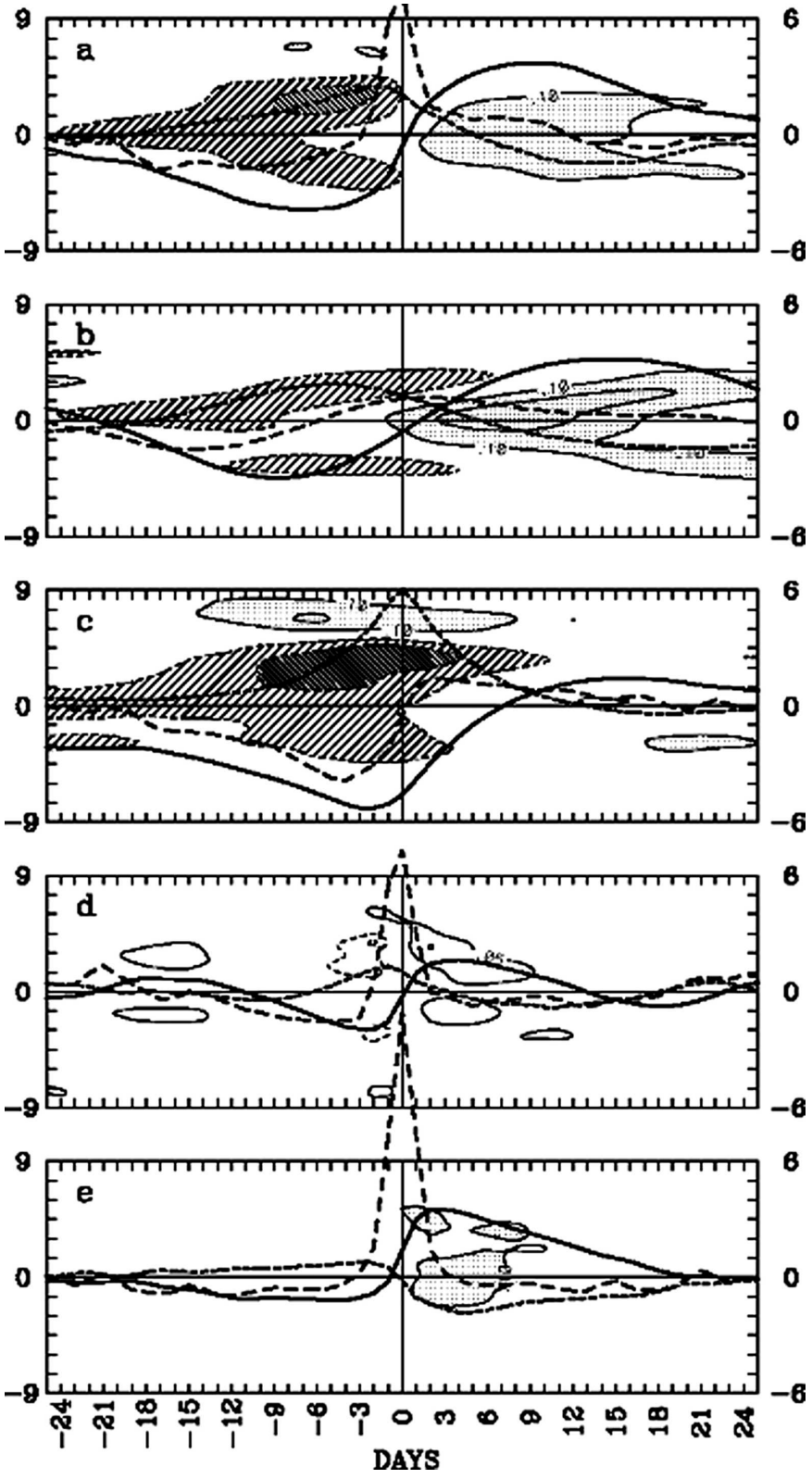
a
b
c
d
e
9
0
−9
6
−6
−24
−21
−18
−15
−12
−9
−6
−3
0
3
6
9
12
15
18
21
24
DAYS

western Pacific and global AAM has a large positive time tendency, at which time equatorial westerlies are already present over the Western Hemisphere. In sequence 2 (Fig. 11), a negative Pacific–North American teleconnection pattern (W03) develops by day −2 as Rossby waves disperse across Asia and then North America during the 18-day sequence; this contributes to a large positive frictional torque anomaly at day 0 (not shown). In sequence 3 (Fig. 12), rapid energy dispersion events (30 m s^{-1}) are seen centered over the East Asian, North American, and South American mountains at day 0 and contribute to a positive global mountain torque anomaly. The events are embedded in a pattern of wavenumber 0–2 zonal wind anomalies, some of which are highlighted by arrows. Four days after the positive torque, westerly flow anomalies extend from the equatorial east Pacific eastward and poleward to the midlatitude central Pacific. These anomalies represent the ~20-day quasi-oscillatory component of the GSDM (see also Fig. 9d).

Interestingly, sequences 1–3 all have local statistically significant wind and SLP anomalies in tropical regions, even the two faster modes of variability. The features are characterized by wavenumber 0–1 zonal wind anomalies at upper levels and provide a synoptic pattern that links the different types of subseasonal variability. This complements and extends the results for the global and zonal AAM relationship that is the basis for the model.

c. The synoptic–dynamic model (GSDM)

Figure 13 shows the 4 stages of the GSDM nominally centered about 12 days apart with an ~50-day oscillation due to the MJO. These numbers have a wide range since the subseasonal band is broad, and transition between phases can occur rapidly. A complete temporal evolution of anomalies is shown only for the MJO. Twenty-two maps representing 11 lags for both OLR EOF 1 and EOF 2 were examined and the 4 lags in Fig. 13 were chosen to represent the MJO. The EOFs are in quadrature and show similar patterns when shifted by ~10 days. Table 2 shows the correspondence between the stages and the lags for the two EOFs. The Hs and Ls for the other components are placed with a specific stage based on the "large AAM tendency" criterion discussed in relation to Fig. 9. Specifically, the colored Hs and Ls shown on sequences 2 (Fig. 11) and 3 (Fig. 12) are used to complete the construction of the stages.

1) STAGE 1

This stage represents a particular phasing of the MJO and the τ_F–τ_M index cycle of the model. Stage 1 and stage 3 are considered the more persistent stages of the GSDM. During stage 1, the anomalous anticyclones linked with the MJO cover most of the tropical Eastern Hemisphere with downstream cyclones over the subtropical west Pacific Ocean. Tropical convection anomalies are consolidated over the eastern Indian Ocean as the MJO convective forcing has intensified from stage 4. In the subtropics, easterly flow anomalies cover the west Pacific and also weakly cover the Atlantic Ocean. The anomalies represent an amplification of the wintertime climatological stationary waves in the Tropics and subtropics (see Fig. 9a of WKS), although the Pacific jet is retracted.

The brown Hs and Ls over the Northern Hemisphere represent the τ_F–τ_M index cycle. A negative PNA pattern is a prominent feature of the wave train disturbance. The circulation centers of this stochastic mode approximately phase with some of the circulation anomalies associated with the MJO. Together, easterly zonal wind anomalies in subtropical latitudes of the Western Hemisphere and in the Tropics of the Eastern Hemisphere lead to the very low relative AAM. As these easterly flow anomalies reach the surface, they lead to a positive frictional torque, which sets the stage for an increase in AAM and a possible transition to stage 2.

Although not depicted in Fig. 9, the general anomalous pattern of synoptic variability is similar to what occurs during La Niña. It involves a northward-shifted storm track and enhanced wave energy propagating into the Tropics. Matthews and Kiladis (1999) show that during this phase of the MJO, the Pacific

←

FIG. 9. The total global atmospheric angular momentum (solid curve), the global mountain torque (long dash curve), and the global frictional torque (short dash curve) anomalies obtained by lag regressions onto various indices using 16 northern winter seasons (November–March 1979–95). The left ordinate labels are Hadleys (1 Hadley = 1.0×10^{18} kg m^2 s^{-2}) and the right labels are AAM units (1 unit = 1.0×10^{24} kg m^2 s^{-1}). The abscissa is lag where negative (positive) values mean the regressed quantity leads (lags) the index. For the contours, the right labels also represent latitude/10 (i.e., 6 = 60°N, etc.). The contour and shading interval is 0.1×10^{24} kg m^2 s^{-1} (the value corresponds to a vertical and zonal mean zonal wind anomaly of 0.3 m s^{-1} at 30°N). The indices used are (a) the daily global AAM tendency, (b) the first EOF of 20–100-day filtered OLR, (c) the global frictional torque minus the MJO, (d) the global relative AAM filtered to retain <30-day periods, and (e) the global mountain torque. The contours start at 0.05×10^{24} kg m^2 s^{-1} in (d).

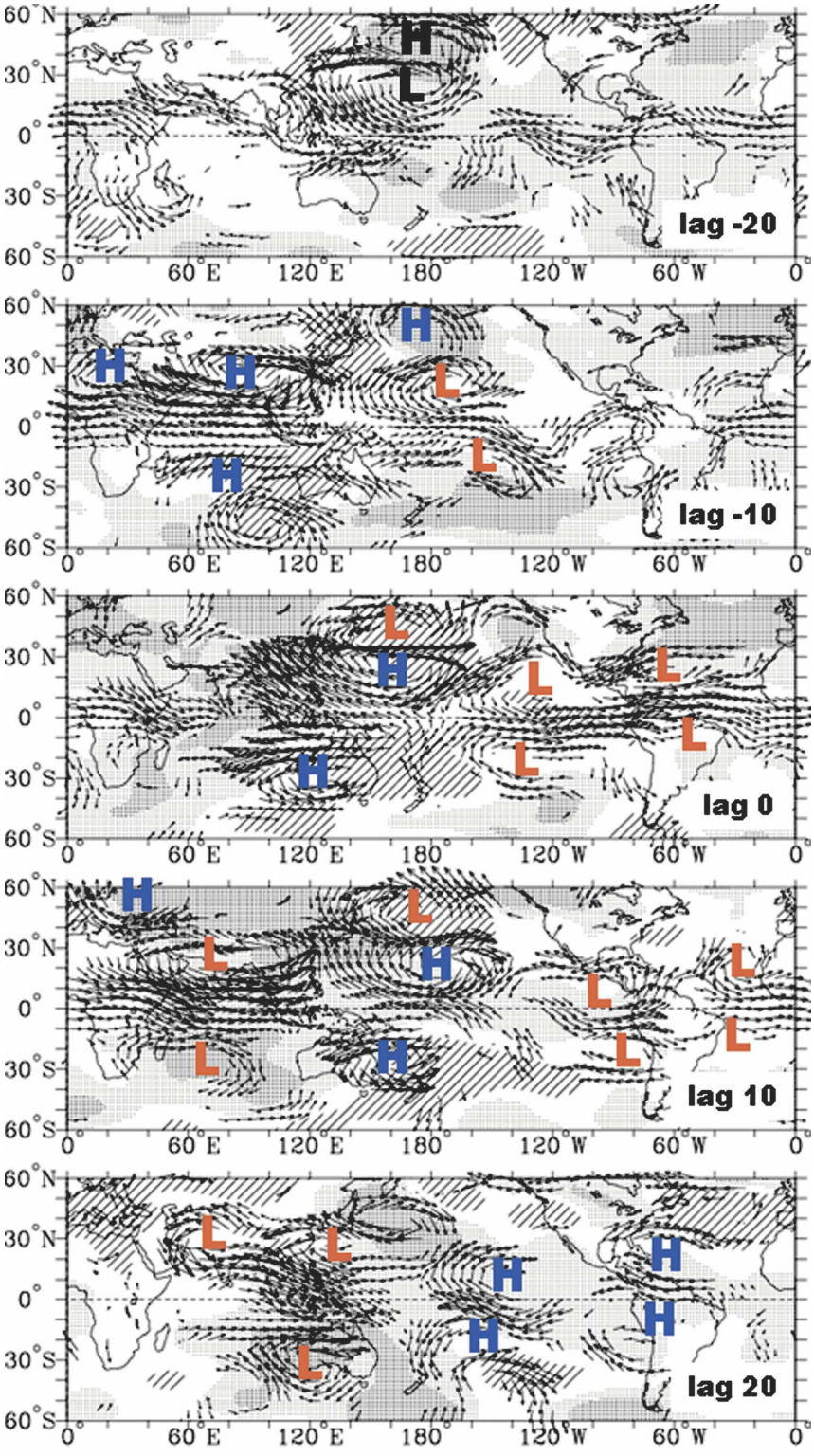

FIG. 10. The 200-mb vector wind (arrows) and SLP anomalies (shading) obtained by lag regression onto EOF 1 of 20–100-day filtered OLR shown in Fig. 8 (top; sequence 1). For the SLP anomalies, stippling (hatched) represents anomalously high (low) pressure. The Hs and Ls depict anticyclonic (cyclonic) 200-mb vector wind anomalies. Only wind anomalies locally significant at 95% are plotted. The red and blue Hs and Ls approximately correspond to the light gray Hs and Ls in Fig. 13 (see also Table 2).

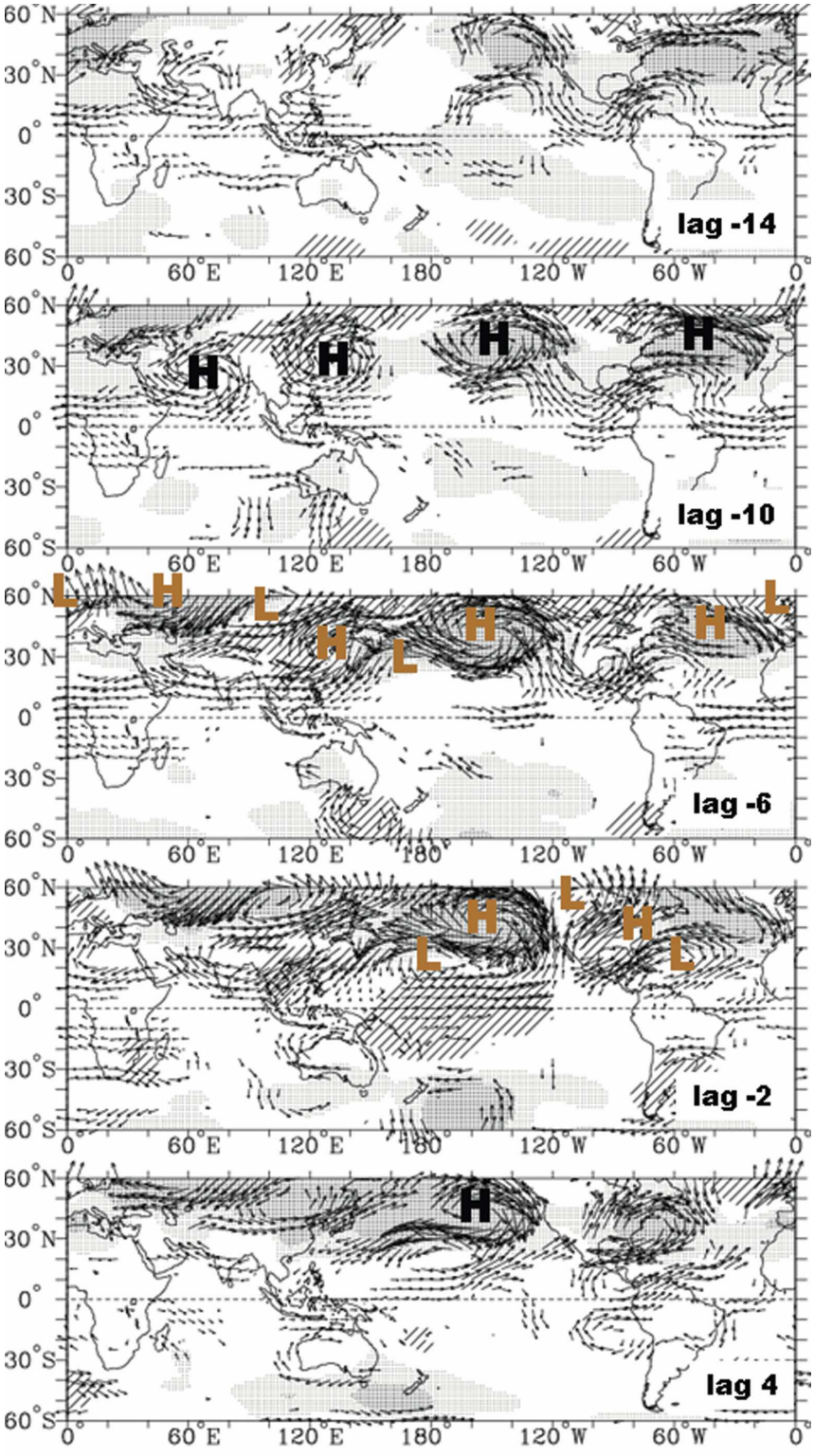

FIG. 11. Same as in Fig. 10 but regressed onto the daily global frictional torque shown in Fig. 8 (middle; sequence 2). The brown Hs and Ls are placed on Fig. 13 as part of stage 1 and stage 3 (opposite phase) of the GSDM.

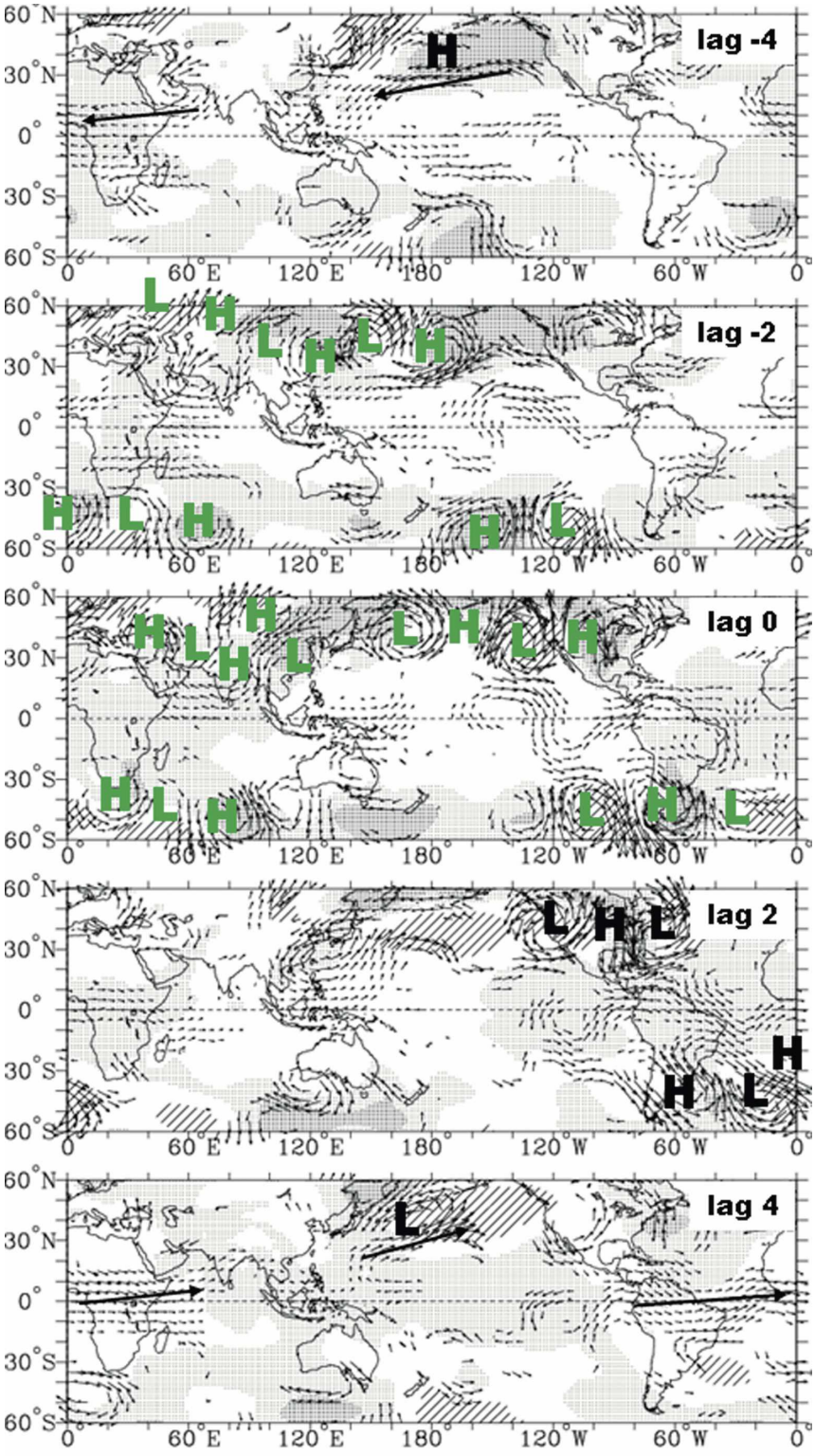

FIG. 12. Same as in Fig. 10 but lag regressions on the <30-day filtered, global relative AAM tendency index given on Fig. 8 (bottom; sequence 3). The green Hs and Ls are placed on Fig. 13 as part of stage 2 and stage 4 (opposite phase) of the GSDM.

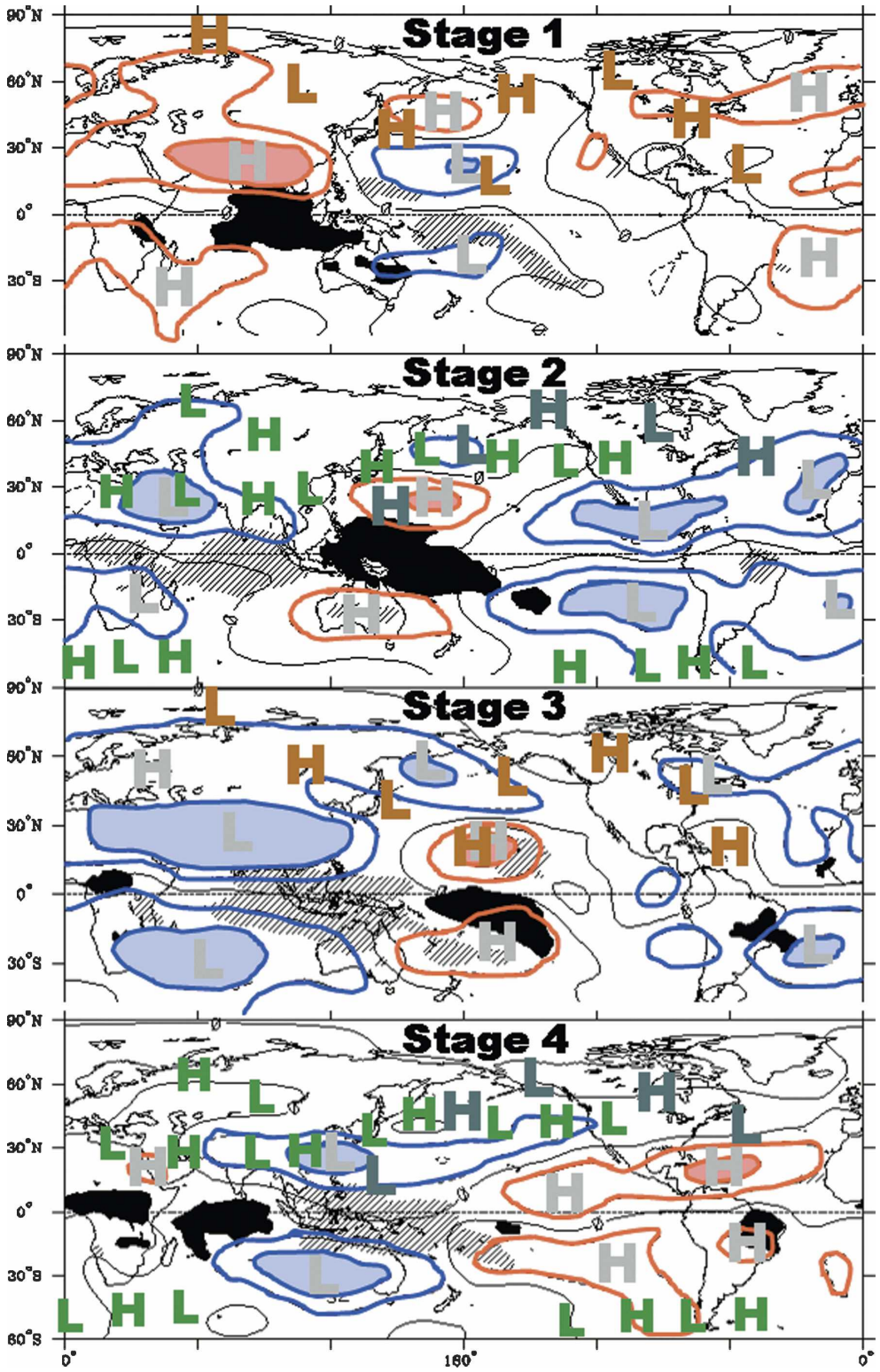

FIG. 13. The four stages of the GSDM of subseasonal variability for the Northern Hemisphere cold season (November–March). The red (blue) isopleths and shading depict subtropical anticyclonic (cyclonic) 200-mb streamfunction anomalies (interhemispheric sign reversal is understood) that accompany MJO tropical convection anomalies as they move east. The black (hatched) shading shows the areas of enhanced (suppressed) convection with the MJO. The Hs and Ls are used to show the associated anomalous anticyclonic (or high pressure) and cyclonic (or low pressure) gyres. The lighter gray Hs and Ls are for the MJO while the heavier gray ones illustrate a west Pacific wave train linked to the MJO at stage 2. The brown Hs and Ls depict teleconnection patterns associated with the frictional torque and the green ones show synoptic-scale wave trains.

TABLE 2. GSDM stages and their relation to OLR EOF 1 and EOF 2. The "OLR EOF and lag" column contains the EOFs and lags that make up the MJO contribution to the four stages, as depicted in Fig. 13. None of these are shown explicitly in Fig. 10, which shows regressions onto EOF1 only.

Stage	OLR EOF and lag	Lag of other EOF	Fig. 10 shows
1	EOF 1, day −15	EOF 2, day 0	Neither
2	EOF 2, day −10	EOF 1, day 0	c: EOF 1, day 0
3	EOF 2, day 0	EOF 1, day +10	d: EOF 1, day +10
4	EOF 2 day +10	EOF 1, day +20	e: EOF 1, day +20

waveguide tends to be "leakier" since the jet stream is weaker and westerly winds extend over a broad latitudinal band. As wave energy disperses southeastward into the east Pacific ITCZ, the resulting convection anomalies (Kiladis and Weickmann 1997; Matthews and Kiladis 1999) can lead to subtropical jets that combine with the western United States trough and produce baroclinic developments over the Great Plains.

Stage 1 can be characterized by an ~weekly variation between strong meridional flow anomalies and strong zonal flow anomalies during northern winter. Transitions from meridional to zonal flows occur in association with baroclinic waves that tend to break anticyclonically over the east Pacific Ocean. Broadly speaking, stage 1 represents a "La Niña" basic state, which has been shown to support greater intraseasonal variance over the North Pacific Ocean (Compo et al. 2001) and life cycle 1 (LC1; anticyclonic) of baroclinic wave activity (Shapiro et al. 2001).

2) STAGE 2

Stage 2 represents a transitional phase of the GSDM where the MJO moves into the Pacific Ocean region and synoptic-scale energy dispersion contributes to strong positive mountain torques. Positive MJO convection anomalies that were previously centered west of 120°E now set up over the western Pacific at around 150°E. Weickmann and Khalsa (1990) have shown that this transition can occur rapidly in association with high-frequency tropical transients since identified as convectively coupled equatorial Kelvin waves by Wheeler and Kiladis (1999). The MJO circulation anomalies are also transitional as twin anticyclones move into the western Pacific and twin cyclones cover the remainder of the Tropics including the western Indian Ocean. The anomaly pattern represents an eastward shift of the climatological flow in the Tropics and subtropics (see Fig. 9b of WKS).

The green Hs and Ls are the fast time-scale patterns that give a large positive mountain torque and precede stronger westerly flow in the subtropics from 10–30-day oscillations. In the Northern Hemisphere, two wave trains over Asia meet over the west Pacific and disperse downstream. In the Southern Hemisphere, wave trains are shown that produce positive mountain torques over the South American Andes and the African highlands.

Stage 2 often represents a sudden transition to new tropical heat sources, and considerable transient Rossby wave activity emanates from the new sources over the east Indian and the west Pacific Oceans. Over the west Pacific Ocean, this is characterized by the spinup of upper-level anticyclones, whose circulation then interacts with midlatitude weather systems. One such interaction can initiate a growing Pacific Ocean wave train (the heavy gray Hs and Ls) that extends downstream across North America. Although the wave train is depicted in stage 2, it is best developed 6–10 days after convection moves into the western Pacific Ocean region. In that case, the green Hs and Ls are precursors to the dark gray Hs and Ls.

WNS obtain a similar wave train in their study of the response to tropical heating. The initial state of their singular vector 2 (SV2) would project onto both the convection and green circulation centers shown at stage 2. The gray Hs and Ls emanating from the tropical west Pacific Ocean region represent the final state of SV2. Other studies of MJO composite circulation anomalies (e.g., Knutson and Weickmann 1987) find a similar feature. The wave train is seldom a simple Rossby wave dispersing from a tropical heat source (Hoskins and Karoly 1981; Sardeshmukh and Hoskins 1988) but often involves tropical–extratropical interaction on fast time scales.

3) STAGE 3

As the GSDM convection anomaly moves eastward, the circulation anomalies now act to weaken the normal wintertime climatological flow in the Tropics and subtropics (see Fig. 9c of WKS), but at the same time extend and strengthen the jet across the Pacific Ocean. The brown Hs and Ls connecting Asia and North America now project on a positive PNA. Strong westerly flow occurs at 35°N over the Western Hemisphere and in the Tropics over the Eastern Hemisphere, from the combination of the MJO and the intermediate time-scale $\tau_F - \tau_M$ index cycle. The storm track is farther south over the Pacific and can give rise to extreme rainfall events along the West Coast. Cyclonic wave breaking is often observed over the east Pacific Ocean, upstream of North America. Stage 3 represents an "El Niño" basic state, and while the patterns are opposite to stage 1, the synoptic variability tends to be less extreme during stage 3.

4) STAGE 4

Stage 4 is similar to stage 2 but with opposite sign and slightly earlier in the MJO life cycle. For example, suppressed convection still covers western Indonesia in stage 4 whereas enhanced convection is farther east at stage 2. The MJO circulation anomalies now produce a westward shift of the wintertime climatological flow in the Tropics and subtropics. Over the Indian Ocean, the strong subtropical cyclones of stage 3 are transitioning to anticyclones as convection redevelops over the central Indian Ocean. This stage has three centers of MJO convection: east of the date line, over South America, and over Africa/west Indian Ocean.

On the synoptic time scale, stage 4 is represented by the sequence of green Ls and Hs, the opposite phase to stage 2. The phase of the south Asian wave train is set by the Indian Ocean convection anomaly located south and east of the anomalous anticyclone at around 60°E. This wave train phases with a separate wave train in the north Asian waveguide (which produces a negative mountain torque there) and then together they disperse east and amplify across the North Pacific toward North America. The combination of a negative mountain and frictional torque from the MJO and a negative mountain torque from the synoptic-scale dispersion leads to a strong negative AAM tendency and sets the stage for decreasing westerly flow in the atmosphere.

d. The combined AAM cycle

Much is known about the subseasonal budget of global and zonal AAM based on recent diagnostic studies using reanalysis data. For the global budget, Weickmann et al. (2000) and Egger and Hoinka (2002) show that the mountain torques force AAM anomalies and the frictional torque damps them. In the semantics of Fourier analysis, this means the friction torque leads the mountain torque. All subseasonal variability has this characteristic. The zonal budget brings in the role of AAM transports, which are zero in a global integral. Meridional transports provide a link back to the structure and orientation of troughs and ridges within the spatial patterns shown in Fig. 13. Subseasonal zonal AAM anomalies have well-developed poleward (Feldstein 2001) and downward propagation that extends from the equatorial tropopause to the subtropical solid earth (Egger and Weickmann 2007; Egger and Hoinka 2005). Dynamically, many questions remain about the contribution from different mechanisms in this process. For example, Moncrieff (2004) proposes a role for the vertical transport of zonal momentum due to the structure of organized mesoscale convective complexes. Unfortunately, the zonal AAM budget cannot provide even rudimentary answers because it is not balanced in either the NCEP–National Center for Atmospheric Research (NCAR) (WKS) nor the European Centre for Medium-Range Weather Forecasts (ECMWF) reanalyses (Egger and Hoinka 2005). The zonal mean flux convergence of relative AAM is large compared to the sum of zonal mean torques, even when the Coriolis and gravity wave drag torques are included. This contributes to a systematic dipole error in the zonal AAM budget as shown by W03 (see his Figs. 3c,d).

In this section, we are not so much interested in the AAM budget as in using it to bring out additional features of the GSDM and to relate its spatial patterns in Fig. 13 with the combined AAM cycle. Some of the features of the cycle are summarized in Table 3. Figure 14 shows the lag regression of the global and zonal AAM, the flux convergence of AAM, and the mountain and frictional torque onto daily time series of the global relative AAM tendency for November–March 1979–95. The approximate locations of the GSDM stages are shown at the bottom of the figure.

In Fig. 13, the Hs and Ls from different time scales were placed on the four stages without considering the actual time behavior that might ensue. Figure 14 shows this in an average sense for the global and zonal mean fields by regressing on an index that contains all the components of the GSDM (i.e., the daily global relative AAM tendency). The time behavior is clearly asymmetric with respect to zero lag, as would be expected, if only because of the intermediate time scale τ_F–τ_M index cycle. There appears to be a buildup phase during stage 1 (see Fig. 14 prior to day −5) where several processes are persistent, and there is a gradual decrease (increase) in relative AAM (frictional torque) anomaly due to a negative mountain torque. This occurs early in the MJO's life cycle when positive convection anomalies are over the Indian Ocean and the intermediate time scale contributes a negative PNA as positive frictional torques increase (Fig. 14c).

There then appears an abrupt reversal or weakening in all anomalies around day −2, arguably led by a reversal in the meridional AAM transport across 30°N, from poleward before to equatorward after. This occurs just as the zonal mean easterly flow anomalies in the subtropics reach their peak values at 25°N. At the same time, the dominate wave train in the GSDM shifts from the intermediate time-scale teleconnection type (stage 1) to the wave-packet-dominated fast time-scale type (stage 2). The latter helps reverse the mountain torque and possibly initiates the "flip" in meridional transports. Figure 14b has a momentum source due to transports that extends from the northern to southern sub-

TABLE 3. Summary of the GSDM stages.

	Characteristics
Stage 1	MJO convection around 110°E with enhanced (suppressed) tropical convective forcing across the eastern (western) hemisphere
	Amplified (tropical/subtropical) seasonal base state
	Low AAM/strengthened subtropical momentum sink
	PNA < 0 forced by τ_F–τ_M index cycle ($\tau_M < 0$, $\tau_F > 0$ sequence)
	Contracted East Asian and North American jets, displaced poleward/split flows over the oceans
	The MJO and τ_F–τ_M index cycle give large positive frictional torques
	La Niña–like base state with Pacific Ocean anticyclonic wave breaking
	Wave energy dispersion favors high-impact weather across the U.S. plains
Stage 2	MJO convection around 150°E
	Eastward-shifted seasonal base state
	d(AAM)/dt >0 and momentum sink shifting poleward
	The MJO and fast time-scale component give large positive mountain torques
	Western Pacific–North American Rossby wave train; strong ridge from U.S. West Coast into Alaska
	Asian–Pacific wave train favors east Pacific cyclonic wave break for transition to stage 3
	Much below normal temperatures possible across central and eastern United States
Stage 3	MJO convection around date line with enhanced (suppressed) tropical convective signal across the western (eastern) hemisphere
	Deamplified seasonal base state
	High AAM/weakened subtropical momentum sink
	PNA > 0 forced by mountain torque > 0, friction torque < 0 sequence
	Extended East Asian and North American jets, displaced equatorward/split flows across the continents
	The MJO and τ_F-τ_M index cycle give large negative frictional torques
	El Niño–like base state with east Pacific Ocean cyclonic wave breaking
	High-impact weather event possible along the West Coast
Stage 4	MJO convective signal across the Western Hemisphere, locations at ~160°W, 60°W, and 60°E
	Westward-shifted seasonal base state
	d(AAM)/dt <0/weakened momentum sink shifting poleward
	MJO and fast component give large negative mountain torque
	Strong subtropical jets over the Western Hemisphere
	Asian–Pacific wave train favors anticyclonic wave break across east Pacific Ocean for transition to stage 1
	Heavy precipitation event possible across southwestern United States

tropics. The MJO is also undergoing a transition at this time when tropical convection moves out of the Indian Ocean and into the west Pacific Ocean region. A further forcing of the torques by the MJO could then lead to a continued oscillation. Figure 14a shows more damped anomalies after day 0 again reflecting the τ_F–τ_M index cycle.

During an oscillation, the vertically integrated AAM anomaly (Fig. 14a) alternates between easterly and westerly flow anomalies that propagate from equatorial regions to the subtropics. The oscillation represents the MJO along with a sharpening of the curve by 10–30-day variations. Global angular momentum is at a minimum at stage 1 when negative AAM anomalies (easterly wind anomalies) are moving off the equator and tropical sea level pressure is low. By stage 2, the easterly anomalies are approaching the subtropics and weakening on the equator. Tropical SLP is on the rise and MJO convection is active over the western Pacific. By stage 3, westerly flow anomalies are lifting off the equator, tropical SLP is high, and global AAM reaches a maximum. Convection is near the date line, but it is strongly suppressed over the Indian Ocean from both the MJO and 10–30-day oscillations. The cycle ends with stage 4 as westerly wind anomalies move off the equator and convection is active in the three separate centers.

The frictional torque tends to be large during stages 1/2 and 3, when anomalies are more persistent than during stages 2 and 4. Synoptically, stage 1 is represented by strong trade winds and a northward-shifted westerly flow, especially over the Atlantic and Pacific Oceans. Sometimes, blocking can contribute to the torque through easterly flow anomalies that are large and farther north. The mountain torque tends to be large during stages 2 and 4, which also tend to be more transient with faster time scales involved. The positive mountain torque in the Southern Hemisphere is due to the Andes and develops as convection shifts into the western Pacific between stages 1 and 2 (Madden and Julian 1972; Milliff and Madden 1996). In the Northern

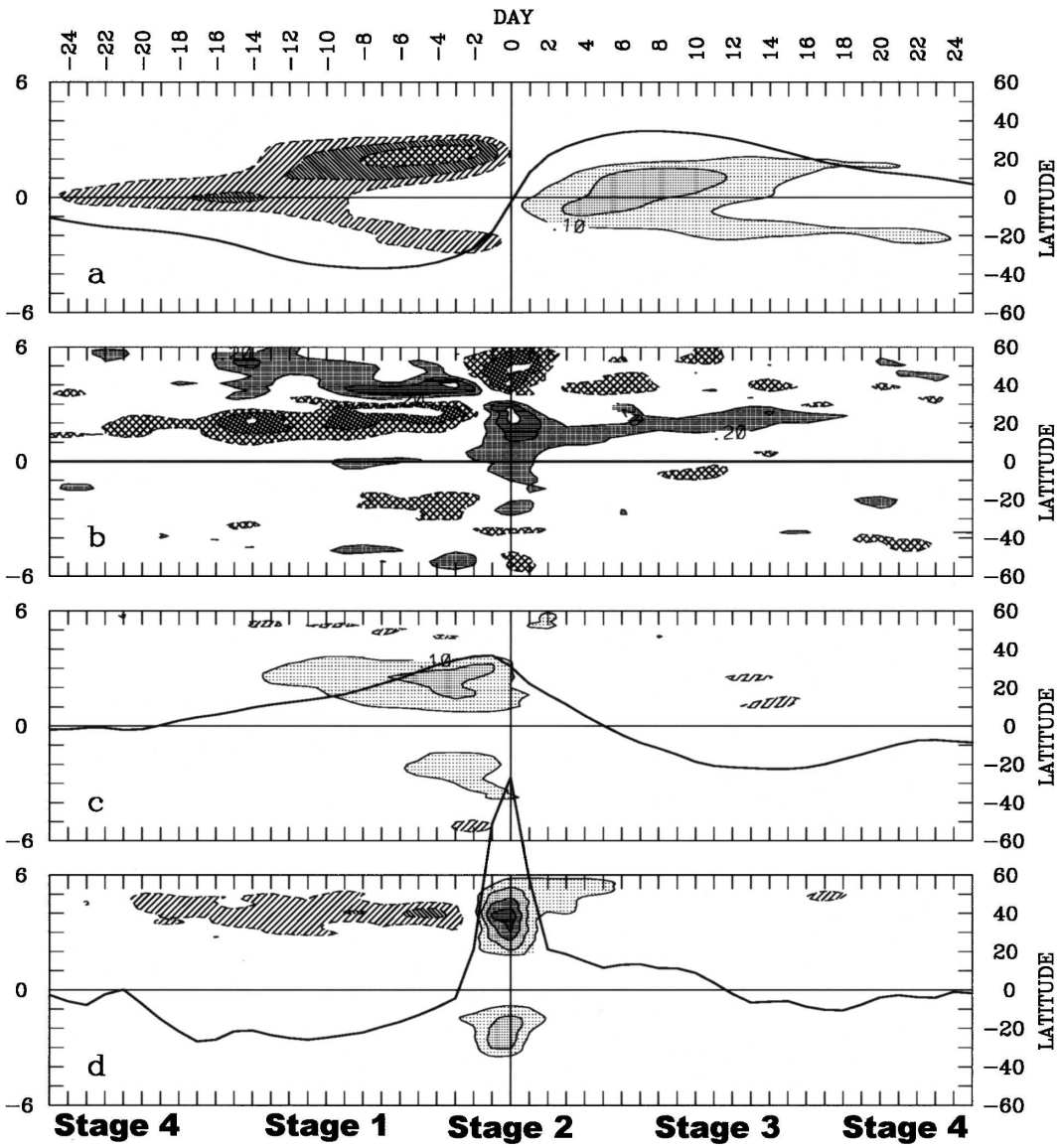

FIG. 14. Zonal (contours and shading) and global (curves) anomalies obtained by lag regression onto the daily relative AAM tendency for November–March 1979–95. (a) Total AAM: contour interval is 0.1×10^{24} kg m^2 s^{-1}, left ordinate labels are for global curve in AAM units (1 unit = 1.0×10^{24} kg m^2 s^{-1}). (b) The flux convergence of relative AAM: contour/shading interval is 0.2 Hadleys, left ordinate labels are Hadleys. (c) The frictional torque: same as in (b) but contour–shading interval is 0.1 Hadleys. (d) Same as in (c) but for mountain torque. Note that the contour interval in (b) is twice that in (c), (d). The right ordinate labels are latitude for the zonal contours.

Hemisphere, the positive mountain torque is produced by high pressure anomalies east of the Tibetan Plateau and cold air outbreaks that accompany the shift of convection to the west Pacific.

4. Summary and conclusions

We have proposed a synoptic–dynamic model of subseasonal variability that is useful for weather climate monitoring and for medium-range prediction assessment. The monitoring involves daily subseasonal variability while the prediction focuses on forecast lead times from 3 days to 3 weeks. The GSDM is constructed for the Northern Hemisphere cool season but the same processes are active during the rest of the seasonal cycle. For example, to first order, the MJO circulation and convective anomalies merely shift northwest during northern summer and become larger in the Southern (winter) Hemisphere. There is also a summer analog to the stage 2 wave train seen in Fig. 13. The approach

discussed in section 3 will be applied to the other seasons in future work. Newman and Sardeshmukh (1998) provide some clues about the sensitivity of forcing and response during the course of the seasonal cycle.

By keying in on the global relative AAM tendency, the construction of the GSDM is made easier, although the regional anomaly patterns and their relationships are blurred. A version of Fig. 13 (not shown) made from the lag regression of the 200-mb streamfunction and OLR fields onto the daily AAM tendency supports the idea that the composite variations around day 0 (stage 2) consist of different time scales of forcing, sometimes contributing to large global AAM tendencies. In our approach, we have defined the dominant time scales that drive the global AAM tendency and then the preferred phase relationships that give a large time tendency. As a result, stages 2 and 4 contain a specific phase of the fast time-scale component whereas only general storm-track changes are invoked in stages 1 and 3.

The GSDM is used in conjunction with the daily real-time monitoring of a broad range of weather climate indices, maps, and forecasts. These range from the large-scale patterns of SST down to ongoing baroclinic life cycles or tropical convectively coupled Kelvin waves. The multiple time scales contribute to rapid transitions of the tropical and extratropical circulation, which are difficult for operational GCMs to capture and can lead to large forecast errors. The 2001–02 case study examined two such transitions and their relationship to tropical forcing from two MJOs and midlatitude mountain torques. It highlighted a link between the MJO, extratropical wave trains, and baroclinic wave processes over the Pacific–North American region. The transition included a cyclonic (anticyclonic) wave break that ushered in strong (weaker) subtropical westerlies and a positive (negative) PNA.

An operational forecast model's 11-day prediction showed that the 3 periods of relatively low model skill in 150-mb streamfunction at 11 days occur when a major longitudinal shift of tropical convection is observed during the period of the forecast. The model is more successful at capturing the initial conditions of tropical precipitation and persisting them—a sometimes useful attribute for the week 1 forecast. The relationship between objectively defined "flare-ups" of convection and the time evolution of predicted and observed fields will be examined in a longer reforecast dataset in future work.

The GSDM was developed to provide an additional tool for the medium-range forecaster to assess the state of the atmosphere–ocean at the initial time and thereby evaluate the predictions of numerical models. The GSDM is being used in real-time weather climate discussions and experimental week 1–3 predictions (available online at http://www.cdc.noaa.gov/MJO/Forecasts/climate_discussions.html). Whether the GSDM can be used to improve subseasonal predictions on average remains to be determined. However, real-time weather climate monitoring within the framework of the GSDM should help capture sudden shifts in tropical convective forcing and may improve the interpretation of numerical model predictions of high-impact, extreme weather events.

Acknowledgments. Thanks to Brian Mapes and two anonymous reviewers for their thoughtful and constructive comments on the paper. We thank Randy Dole for his encouragement and support as director of the Climate Diagnostics Center. Thanks to Dennis H. McCarthy, Director of the NOAA/NWS Office of Climate, Weather, and Water Services, for supporting E. Berry's temporary assignment to CDC to work on the paper. We also recognize Peter A. Browning, Chief of the NWS Central Region Headquarters Meteorological Sciences Division, for supporting additional travel to CDC to finish the final manuscript and Larry Ruthi, Meteorologist in Charge for the NWS Weather Forecast Office, for allowing E. Berry the time and support needed to complete this project.

REFERENCES

Bjerknes, J., 1919: On the structure of moving cyclones. *Geofys. Publ.,* **1,** 1–8.

Branstator, G. W., 1987: A striking example of the atmosphere's leading traveling pattern. *J. Atmos. Sci.,* **44,** 2310–2323.

——, 1992: The maintenance of low-frequency atmospheric anomalies. *J. Atmos. Sci.,* **49,** 1924–1945.

Chang, E. K. M., 1993: Downstream development of baroclinic waves as inferred from regression analysis. *J. Atmos. Sci.,* **50,** 2038–2053.

——, 1999a: Characteristics of wave packets in the upper troposphere. Part I: Northern Hemisphere winter. *J. Atmos. Sci.,* **56,** 1708–1728.

——, 1999b: Characteristics of wave packets in the upper troposphere. Part II: Seasonal and hemisphere variations. *J. Atmos. Sci.,* **56,** 1729–1747.

——, 2005: The impact of wave packets propagating across Asia on Pacific cyclone development. *Mon. Wea. Rev.,* **133,** 1998–2015.

Charney, J., and J. DeVore, 1979: Multiple flow equilibria and blocking. *J. Atmos. Sci.,* **36,** 1205–1216.

Compo, G. P., P. D. Sardeshmukh, and C. Penland, 2001: Changes of subseasonal variability associated with El Niño. *J. Climate,* **14,** 3356–3374.

Dole, R. M., 1986: The life cycles of persistent anomalies and blocking over the North Pacific. *Advances in Geophysics,* Vol. 29, Academic Press, 31–69.

——, 2007: Linking weather and climate. *Frederick Sanders Symposium,* L. Bosart and H. Bluestein, Eds., Amer. Meteor. Soc., in press.

Egger, J., and K. P. Hoinka, 2002: Covariance analysis of the global atmospheric axial angular momentum budget. *Mon. Wea. Rev.,* **130,** 1063–1070.

——, and ——, 2005: Torques and the related meridional and vertical fluxes of axial angular momentum. *Mon. Wea. Rev.,* **133,** 621–633.

——, and K. M. Weickmann, 2007: Latitude–height structure of the atmospheric angular momentum cycle associated with the Madden–Julian oscillation. *Mon. Wea. Rev.,* in press.

Feldstein, S. B., 2000: The timescale, power spectra, and climate noise properties of teleconnection patterns. *J. Climate,* **13,** 4430–4440.

——, 2001: Friction torque dynamics associated with intraseasonal length-of-day variability. *J. Atmos. Sci.,* **58,** 2942–2953.

Franzke, C., S. Lee, and S. B. Feldstein, 2004: Is the North Atlantic Oscillation a breaking wave? *J. Atmos. Sci.,* **61,** 145–160.

Hamill, T. M., J. S. Whitaker, and X. Wei, 2004: Ensemble reforecasting: Improving medium-range forecast skill using retrospective forecasts. *Mon. Wea. Rev.,* **132,** 1434–1447.

Hartmann, D. L., M. L. Michelsen, and S. A. Klein, 1992: Seasonal variations of tropical intraseasonal oscillations: A 20–25-day oscillation in the western Pacific. *J. Atmos. Sci.,* **49,** 1277–1289.

Hoskins, B. J., and D. J. Karoly, 1981: The steady linear response of a spherical atmosphere to thermal and orographic forcing. *J. Atmos. Sci.,* **38,** 1179–1196.

——, and T. Ambrizzi, 1993: Rossby wave propagation on a realistic longitudinally varying flow. *J. Atmos. Sci.,* **50,** 1661–1671.

Kiladis, G. N., and K. M. Weickmann, 1997: Horizontal structure and seasonality of large-scale circulations associated with submonthly tropical convection. *Mon. Wea. Rev.,* **125,** 1997–2013.

Knutson, T. R., and K. M. Weickmann, 1987: 30–60 day atmospheric oscillations: Composite life cycles of convection and circulation anomalies. *Mon. Wea. Rev.,* **115,** 1407–1436.

Lin, J. L., and Coauthors, 2006: Tropical intraseasonal variability in 14 IPCC AR4 climate models. Part I: Convective signals. *J. Climate,* **19,** 2665–2690.

Lorenz, D. J., and D. L. Hartmann, 2003: Eddy–zonal flow feedback in the Northern Hemisphere winter. *J. Climate,* **16,** 1212–1227.

Lott, F., and F. D'Andrea, 2005: Mass and wind axial angular-momentum responses to mountain torques in the 1–25 day band: Links with the Arctic Oscillation. *Quart. J. Roy. Meteor. Soc.,* **131,** 1483–1500.

——, A. W. Robertson, and M. Ghil, 2001: Mountain torques and atmospheric oscillations. *Geophys. Res. Lett.,* **28,** 1207–1210.

Madden, R. A., and P. R. Julian, 1971: Detection of a 40–50 day oscillation in the zonal wind. *J. Atmos. Sci.,* **28,** 702–708.

——, and ——, 1972: Description of global-scale circulation cells in the tropics with a 40–50 day period. *J. Atmos. Sci.,* **29,** 1109–1123.

——, and ——, 1994: Observations of the 40–50-day tropical oscillation—A review. *Mon. Wea. Rev.,* **122,** 814–837.

Matthews, A. J., and G. N. Kiladis, 1999: The tropical–extratropical interaction between high-frequency transients and the Madden–Julian oscillation. *Mon. Wea. Rev.,* **127,** 661–677.

Milliff, R. F., and R. A. Madden, 1996: The existence and vertical structure of fast, eastward moving disturbances in the equatorial troposphere. *J. Atmos. Sci.,* **53,** 586–597.

Mo, K. C., 1999: Alternating wet and dry episodes over California and intraseasonal oscillations. *Mon. Wea. Rev.,* **127,** 2759–2776.

——, 2001: Adoptive filtering and prediction of intraseasonal oscillations. *Mon. Wea. Rev.,* **129,** 802–817.

Moncrieff, M. W., 2004: Analytic representation of the large-scale organization of tropical convection. *J. Atmos. Sci.,* **61,** 1521–1538.

Namias, J., 1954: Quasi-periodic cyclogenesis in relation to the general circulation. *Tellus,* **6,** 8–22.

Newman, M., and P. D. Sardeshmukh, 1998: The impact of the annual cycle on the North Pacific/North American response to remote low frequency forcing. *J. Atmos. Sci.,* **55,** 1336–1353.

——, ——, and C. Penland, 1997: Stochastic forcing of the wintertime extratropical flow. *J. Atmos. Sci.,* **54,** 435–455.

——, ——, C. R. Winkler, and J. S. Whitaker, 2003: A study of subseasonal predictability. *Mon. Wea. Rev.,* **131,** 1715–1732.

Nielsen-Gammon, J. W., 2001: A visualization of the global dynamic tropopause. *Bull. Amer. Meteor. Soc.,* **82,** 1151–1167.

Peixoto, J., and A. Oort, 1992: *Physics of Climate*. American Institute of Physics, 520 pp.

Rossby, C. G., 1941: The scientific basis of modern meteorology. *Climate and Man: Yearbook of Agriculture,* United States Department of Agriculture, United States Printing Office, 599–655.

Sardeshmukh, P. D., and B. J. Hoskins, 1988: The generation of global rotational flow by steady idealized tropical divergence. *J. Atmos. Sci.,* **45,** 1228–1251.

——, M. Newman, and M. D. Borges, 1997: Free barotropic Rossby wave dynamics of the wintertime low-frequency flow. *J. Atmos. Sci.,* **54,** 5–23.

Shapiro, M. A., and S. Gronas, Eds., 1999*: The Life Cycles of Extratropical Cyclones.* Amer. Meteor. Soc., 359 pp.

——, H. Wernli, N. A. Bond, and R. Langland, 2001: The influence of the 1997–1999 ENSO on extratropical baroclinic life cycles over the eastern North Pacific. *Quart. J. Roy. Meteor. Soc.,* **127,** 331–342.

Simmons, A. J., and B. J. Hoskins, 1978: The lifecycles of some nonlinear baroclinic waves. *J. Atmos. Sci.,* **35,** 414–432.

——, and ——, 1979: The downstream and upstream development of unstable baroclinic waves. *J. Atmos. Sci.,* **36,** 1239–1254.

——, and ——, 1980: Barotropic influences on the growth and decay of nonlinear baroclinic waves. *J. Atmos. Sci.,* **37,** 1679–1684.

——, and A. Hollingsworth, 2002: Some aspects of the improvement in skill of numerical weather prediction. *Quart. J. Roy. Meteor. Soc.,* **128,** 647–677.

——, J. M. Wallace, and G. W. Branstator, 1983: Barotropic wave propagation and instability, and atmospheric teleconnection patterns. *J. Atmos. Sci.,* **40,** 1363–1392.

Smagorinsky, J., 1967: The role of numerical modeling. *Bull. Amer. Meteor. Soc.,* **48,** 89–93.

Thompson, D. W. J., and J. M. Wallace, 2000: Annular modes in the extratropical circulation. Part I: Month-to-month variability. *J. Climate,* **13,** 1000–1016.

Thorncroft, C. D., B. J. Hoskins, and M. E. McIntyre, 1993: Two paradigms of baroclinic-wave life-cycle behaviour. *Quart. J. Roy. Meteor. Soc.,* **119,** 17–55.

Wallace, J. M., and D. S. Gutzler, 1981: Teleconnections in the geopotential height field during the Northern Hemisphere winter. *Mon. Wea. Rev.,* **109,** 784–812.

Weickmann, K. M., 2003: Mountains, the global frictional torque, and the circulation over the Pacific–North American region. *Mon. Wea. Rev.,* **131,** 2608–2622.

——, and S. J. S. Khalsa, 1990: The shift of convection from the Indian Ocean to the western Pacific Ocean during a 30–60 day oscillation. *Mon. Wea. Rev.,* **118,** 964–978.

——, G. N. Kiladis, and P. D. Sardeshmukh, 1997: The dynamics of intraseasonal atmospheric angular momentum oscillations. *J. Atmos. Sci.,* **54,** 1445–1461.

——, W. A. Robinson, and C. Penland, 2000: Stochastic and oscillatory forcing of global atmospheric angular momentum. *J. Geophys. Res.,* **105,** 15 543–15 557.

Wheeler, M., and G. N. Kiladis, 1999: Convectively coupled equatorial waves: Analysis of clouds and temperature in the wave number–frequency domain. *J. Atmos. Sci.,* **56,** 374–398.

——, ——, and P. J. Webster, 2000: Large-scale dynamical fields associated with convectively coupled equatorial waves. *J. Atmos. Sci.,* **57,** 613–640.

Whitaker, J. S., and P. D. Sardeshmukh, 1998: A linear theory of extratropical synoptic eddy statistics. *J. Atmos. Sci.,* **55,** 237–258.

Winkler, C. R., M. Newman, and P. D. Sardeshmukh, 2001: A linear model of wintertime low-frequency variability. Part I: Formulation and forecast skill. *J. Climate,* **14,** 4474–4494.